Pergamon

Geochimica et Cosmochimica Acta, Vol. 66, No. 22, pp. 3987–4005, 2002

0016-7037/02 $22.00 + .00

PII S0016-7037(02)00960-2

Platinum-group element geochemistry of peridotite xenoliths from the Sierra Nevada and the Basin and Range, California

CIN-TY AEOLUS LEE*,[a]

Department of Earth Science, MS-126, Rice University, PO Box 1892, Houston, TX 77251-1892

(*Received February* 18, 2002; *accepted in revised form April* 30, 2002)

Abstract—The nature of PGE-Re (PGE = Pt, Pd, Os, Ir, Ru) behavior in subcontinental lithospheric mantle was investigated using new, high precision PGE-Re abundance measurements and previously published Re-Os isotopic analyses of peridotite xenoliths from the Sierra Nevada and Mojave Province, California. Ru/Ir ratios and Ir concentrations are constant over a wide range in S content and major-element fertility indices (e.g., Mg/(Mg+Fe)), indicating that Ru and Ir are not only compatible during partial melting, but also that their partitioning behaviors may not be controlled entirely by sulfide. Pt/Ir, Pd/Ir, Os/Ir, and Re/Ir ratios range from slightly superchondritic to distinctly subchondritic for all xenoliths except for one anomalous sample (1026V), which is characterized by radiogenic $^{187}Os/^{188}Os$, low Re/Os ratio, and large enrichments in Cu, Os, Pt, Pd, and S relative to Ir (COPPS metasomatism). Assuming chondritic initial relative abundances, the magnitudes of some of the depletions in Pt, Pd, Os, and Re relative to Ir and Ru require incompatible behavior or substantial secondary loss. In detail, some samples, which are otherwise characterized by fertile major-element indices, exhibit low S contents and subchondritic Os/Ir and Pd/Ir ratios, indicating that depletions in Pd and Os relative to Ir are not simple functions of the degree of melting as inferred from major elements. Possible mechanisms for depleting Pt, Pd, Os, and Re relative to Ir and Ru include partitioning into chromian spinels and alloys, partitioning between sulfide and sulfide liquids, mobilization by aqueous fluids, or secondary loss associated with late-stage sulfide breakdown. However, it is not possible to explain all of the depletions in Pt, Pd, Os, and Re by any single mechanism.

The preferential enrichment in Os over Re and Ir in sample 1026V is somewhat paradoxical because this sample's radiogenic $^{187}Os/^{188}Os$ requires a metasomatic agent, originating from a source with a high time-integrated Re/Os ratio. The abundant garnet websterite xenoliths may be a suitable source because they have high Re/Os ratios, radiogenic Os, and abundant garnet, which may sequester Re over Os during partial melting. However, their extremely low Os contents require the processing of large amounts of garnet websterite to concentrate enough Os into the metasomatic sulfides needed to enrich sample 1026V in Os. The homogeneity in $^{187}Os/^{188}Os$ ratio in the remaining xenoliths suggest that their Os isotopic compositions were not significantly affected by PGE metasomatism. The singular nature of 1026V's composition emphasizes the rarity of COPPS metasomatism.

1. INTRODUCTION

The siderophile and compatible to moderately incompatible nature of the platinum group elements (PGE = Pt, Ir, Os, Ru, Rh, Pd) and Re makes these elements powerful tools in studying the processes of Earth accretion, core-mantle segregation, and mantle differentiation (Morgan, 1986; Lorand et al., 1993; Brandon et al., 1996, 1998; Pattou et al., 1996; Rehkamper et al., 1997; Snow and Schmidt, 1998; Handler and Bennett, 1999; Puchtel and Humayun, 2000, 2001; Righter et al., 2000; Morgan et al., 2001). In addition, the ^{187}Re-^{187}Os decay system can provide chronologic constraints on the fractionation processes that affect these elements (Walker and Morgan, 1989).

Interpretations of PGE-Re elemental and Re-Os isotopic data in the context of Earth differentiation processes, however, are complicated by an incomplete understanding of the geochemical behaviors of these elements. For example, it has long been accepted that the Earth's upper mantle has an elevated and roughly chondritic PGE-Re abundance pattern and $^{187}Os/^{188}Os$ (Chou, 1978; Morgan, 1986; Meisel et al., 1996; Morgan et al., 2001). The origin of these abundances and signatures is highly debated. Due to their siderophile nature, the PGEs and Re should have partitioned strongly into the metallic core during core formation. A number of hypotheses, such as the addition of a late influx of meteoritic material (Chou, 1978; Morgan, 1986), addition of core material to the mantle (Snow and Schmidt, 1998), inefficient core formation (cf. Jones and Drake, 1986), and lowering of metal-silicate partition coefficients (Brett, 1984; Murthy, 1991) have been suggested. The debate, however, is complicated (or confused) by a growing number of studies, which show that PGE abundance patterns and $^{187}Os/^{188}Os$ ratios in some upper mantle samples deviate from chondritic signatures (Brandon et al., 1996; Pattou et al., 1996; McInnes et al., 1999). Deviations, such as subchondritic Re/Os and Pd/Ir, can generally be explained by a one-stage partial melting event in which Re and Pd are incompatible and Ir and Os are compatible at high degrees of partial melting (Gueddari et al., 1996; Handler and Bennett, 1999). In turn, subchondritic $^{187}Os/^{188}Os$ can be explained by long-term isolation in a low Re/Os environment, as exemplified by subcontinental lithospheric mantle samples, many of which experienced high degrees of melt extraction and long-term chemical and physical isolation in the stable lithosphere (Walker et al., 1989). However, melt-depleted peridotites with near-chondritic

* Author to whom correspondence should be addressed (ctlee@rice.edu).

to superchondritic $^{187}Os/^{188}Os$ and Pd/Ir ratios (Brandon et al., 1996; Pattou et al., 1996; McInnes et al., 1999) cannot be easily explained by a simple partial melting process if Re and Pd are considered incompatible and Ir and Os compatible. These signatures require an initially heterogeneous upper mantle, overprinting by secondary PGE enrichment processes, or more complicated geochemical behaviors of the PGEs during partial melting than currently understood.

The use of PGE-Re and Re-Os isotopic data in studying Earth differentiation processes requires a better understanding of the causes and range in elemental and Os isotopic variations in upper mantle samples (e.g., Morgan et al., 2001). One of the fundamental questions is whether the deviations from chondrite reflect initial mantle heterogeneity or, instead, redistribution processes associated with melt migration (Rehkamper et al., 1999). The approach here is to investigate the geochemical behaviors of Re and the PGEs in the upper mantle in the context of partial melting and re-enrichment processes. The subarc mantle environment may provide an opportunity to study the two processes simultaneously, because recent studies of arc-related peridotites reveal complicated $^{187}Os/^{188}Os$, Re, and PGE systematics (Brandon et al., 1996; McInnes et al., 1999; Peslier et al., 2000). On the one hand, the high degrees of melting that can occur in the mantle wedge should lead to residual peridotites with subchondritic Re/Os, Pt/Ir, and Pd/Ir. Other recent studies have shown that PGE abundance patterns and $^{187}Os/^{188}Os$ in peridotites can be altered by the addition of sulfides (Alard et al., 2000; Luguet et al., 2001) or other metasomatic agents, such as aqueous fluids (Wood, 1987). Given the possibility of pervasive metasomatic overprinting of subarc mantle by melts and aqueous fluids derived from the subducting oceanic crust or recycled sediment, the potential for secondary PGE enrichment processes in subarc mantle exists.

Here, I combine new, high-precision isotope-dilution PGE analyses with previously published Re elemental and Os isotopic analyses (Lee et al., 2000, 2001b) on a suite of peridotite xenoliths sampled along a NW-SE trending transect, extending from the Sierra Nevada to the southern part of the central Basin and Range (Mojave Province) in California (Fig. 1). The Sierra Nevada represents an extinct Mesozoic continental arc associated with the eastward subduction of the Farallon plate beneath the western edge of North America. The Basin and Range is situated in the back-arc region and has been undergoing extension and lithospheric thinning since the mid-Cenozoic. Although much of the Basin and Range may also have been affected by subduction-related metasomatism associated with low-angle subduction between ~70 and 40 Ma ago (Dickinson and Snyder, 1978), the effect of subduction-related metasomatism was probably less here than beneath the Sierra Nevada because of its greater distance from the trench axis. This study was designed to investigate the style and extent of PGE-Re transport in the subarc mantle, to assess the variation of abundance patterns and $^{187}Os/^{188}Os$ ratios with distance from the arc, and to investigate the sources of metasomatic endmembers that might affect PGE-Re and $^{187}Os/^{188}Os$ systematics.

2. XENOLTIH SUITES

2.1. Xenolith Localities

I examined peridotite xenoliths from two localities in the Sierra Nevada and one in the Basin and Range (Fig. 1). Beginning from the west, the first xenolith locality is the late Miocene (8.3 Ma) Big Creek diatreme (BC), which erupted in the central Sierra Nevada just slightly west of the range crest. The xenoliths are not likely to have been subaerially exposed during the emplacement of the diatreme as they come from deep levels in the diatreme. The second site is the Oak Creek flow (OK), associated with the Pleistocene Big Pine volcanic field (~0.115 Ma) in the eastern Sierra Nevada and in the Owens Valley. Outcrops of the Oak Creek basalts are remnants of a larger flow that originated in the high Sierras, and xenoliths were collected from a portion of the flow at the mouth of Oak Creek. The third site is the Pliocene-to-Pleistocene Cima volcanic field, located in the central Mojave Desert Province in southern California. The Cima volcanic field (Ci) consists of more than 70 alkali basalt cinder cones, which formed in two distinct pulses from 7.6 to 3.0 Ma and from 1.0 Ma to the present (Wilshire et al., 1991; Farmer et al., 1995). Cima xenoliths occur as large, subrounded fragments in the cinders of the volcanoes. The Cima xenoliths studied here come from Pleistocene cinder cones.

2.2. Sample Selection and Petrology

2.2.1. Sierra Nevada: Big Creek

Xenoliths at Big Creek consist of garnet-bearing lower crustal xenoliths (granulites, garnet-clinopyroxenites), mantle pyroxenites (garnet websterites), and spinel and garnet peridotites (Dodge et al., 1988; Mukhopadhyay and Manton, 1994; Ducea and Saleeby, 1996, 1998; Lee et al., 2001a). Big Creek peridotite xenoliths range from lherzolites to harzburgites, reflecting variable degrees of melt depletion in the mantle wedge. This is evidenced by olivine Mg#s (Mg# = molar Mg/(Mg+Fe)), ranging from 0.886 (fertile) to 0.914 (depleted), and negative correlations between olivine forsterite content and the amount of TiO_2 and Na_2O in clinopyroxene (Lee et al., 2001a). Nearly all of the peridotites have minerals that are chemically zoned, indicating chemical disequilibrium. The majority of peridotites show evidence for cooling from temperatures as high as 1100°C to temperatures as low as 670°C (based on two pyroxene thermometers; Lee et al., 2001a). A few show evidence for heating on mineral rims. The garnet peridotites yield equilibration pressures up to 3.3 GPa. Mineral chemistry data on these xenoliths are given in Lee et al. (2001a), and petrologic descriptions are given here in Appendix 1. Seven of these peridotites, spanning the entire range of observed fertility, were chosen for PGE analyses. One olivine-bearing garnet websterite (olivine < orthopyroxene < clinopyroxene = garnet), believed to be an upper mantle cumulate or lower crustal residue, was also chosen for PGE analyses.

Visible sulfides are rare or absent from all of these samples except for sample 1026V, which deserves special mention. Visible sulfides in 1026V are abundant and range from

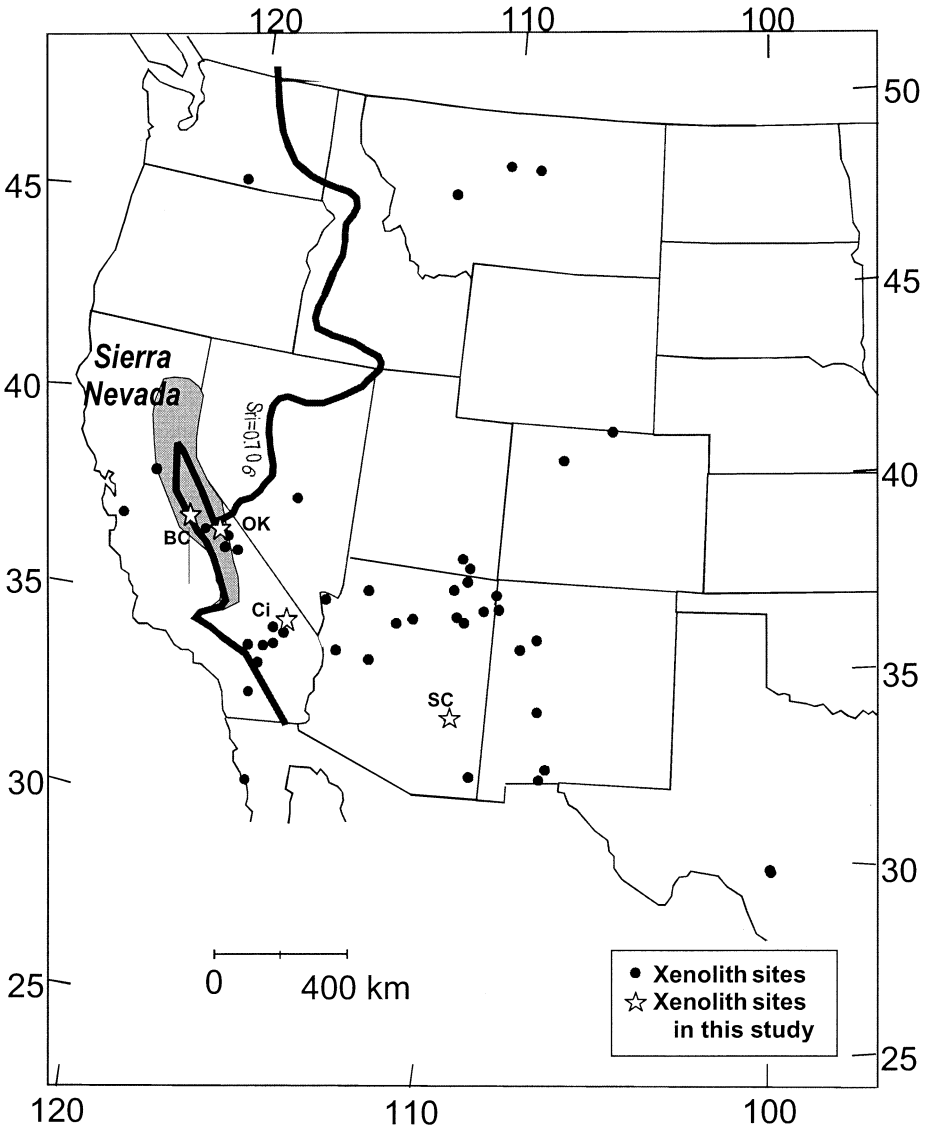

Fig. 1. Map showing the locations of xenolith localities represented in this study (BC = Big Creek; OK = Oak Creek; Ci = Cima). The location from which the in-house standard (SC99-1) was collected is also shown (SC = San Carlos). Thick bold line represents the initial $^{87}Sr/^{86}Sr$ in granitoid rocks and is usually taken as the inferred western edge of the Precambrian craton (Kistler and Peterman, 1973). Gray region labeled Sierra Nevada represents the extent of the Mesozoic Sierran batholith associated with subduction.

$<$ 10 to 200 μm in diameter. The sulfides occur as discrete intergranular grains, as single inclusions in olivine and as series of tiny inclusions in healed olivine fractures (Fig. 2a–d). Those included in olivine or in healed fractures of olivine are represented by monosulfide solid solution (mss), pentlandite, or chalcopyrite compositions (Fig. 3). Intergranular sulfides also consist of mss, pentlandite, and chalcopyrite compositions, but such compositions are invariably preserved within the cores of low-temperature breakdown products, consisting of Fe-oxides and millerite (NiS). Chemical compositions of these sulfides are given in Table A1 of Appendix 1.

2.2.2. Sierra Nevada: Oak Creek

Oak Creek peridotites consist exclusively of spinel lherzolites, Fe-rich dunites, and wehrlites. Garnet-bearing lithologies are entirely absent from this xenolith locality. The Oak Creek peridotites (excluding dunites and wehrlites) are characterized by relatively fertile compositions (Mg# = 0.89–0.90), no chemical zonation in minerals, and equilibration temperatures between 1000 and 1100°C (Lee et al., 2001a). Due to the lack of garnet, Oak Creek peridotites must have been derived from lower pressures (1.5–2 GPa) than the Big Creek peridotites (3 GPa). There are no visible sulfides in the three Oak Creek

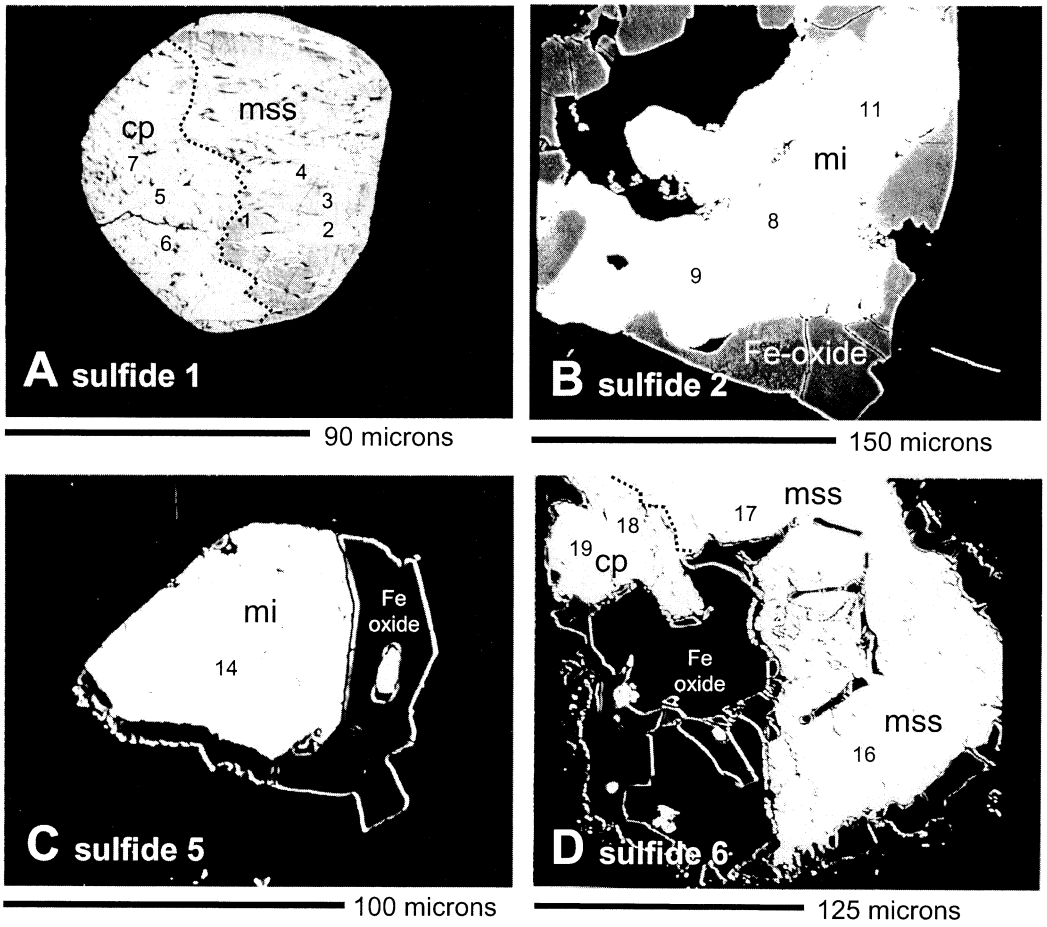

Fig. 2. Back-scattered electron images of sulfides in sample 1026V from Big Creek. This sample is anomalous because of the presence of abundant sulfides. (A) sulfide inclusion in olivine. (B) Intergranular sulfide that has broken down into millerite and Fe-oxides or hydroxides. (C) Intergranular sulfide. (D) Intergranular sulfide. Cp = chalcopyrite; mss = monosulfide solid solution; mi = millerite. Numbers represent electron microprobe analysis points (data shown in Table A1).

peridotites chosen for study, although sulfides have been previously reported in other peridotite xenoliths from the same volcanic field (Ducea and Park, 2000).

2.2.3. Basin and Range: Cima

Cima xenoliths consist of spinel-lherzolites, spinel-harzburgites (uncommon), amphibole-bearing lherzolites, plagioclase-bearing lherzolites, pyroxenites, and gabbros. There are no garnet-bearing lithologies in the Cima xenolith suite. Peridotite Mg#'s range from 0.84 to 0.92, with an average of 0.90 (Lee, 2001; Lee et al., 2001b). Major-element zonation in the minerals is rare or absent. Equilibration temperatures range between 1000 to 1100°C (Lee, 2001; Lee et al., 2001b). Visible sulfides are sparse in Cima peridotites. Four samples spanning fertile to extremely depleted compositions were chosen for study. The most fertile sample (Ki5-139) is a plagioclase lherzolite, while the remaining three are spinel lherzolites or harzburgites. Ki5-16, Ki5-139, and Ki5-32 have been previously investigated for Sr, Nd, and Pb isotopic compositions (Mukasa and Wilshire, 1997).

3. ANALYTICAL TECHNIQUES

3.1. Sulfur Analyses

Sulfur analyses were carried out by K. Sharkey using a Leco spectrophotometer at the University of Leicester, UK. Samples were weighed into a crucible with Fe and W chips added as accelerators to ensure complete combustion of the sample. The crucible was then heated in an RF induction furnace in a stream of O_2 and the sulfur derived as gaseous SO_2 and SO_3. The gases were then passed through a dust filter, drying tube (SO_2 dissolves in water; thus water must be removed), and finally through a catalyst tube to ensure conversion to dioxides. From there, the gases went into the sulfur infrared absorption cell and were passed through another tube that trapped the SO_2 as SO_3. The SO_2 peak was then converted to S values. These values were adjusted for calibration and sample weight to give the final concentration. The values reported here represent the average of two separate analyses for each sample. Blanks (0.3 ppm) and standards were determined in the same manner as samples.

3.2. PGE Analyses by NiS Fusion

Rock samples were crushed and powdered using a ceramic Spex mill to avoid metal contamination. Powders were created from 30 to 50 g of rock for Cima peridotites, from 10 to 20 g of rock for Oak Creek peridotites, and from $<$ 10 g of rock for Big Creek peridotites. Ap-

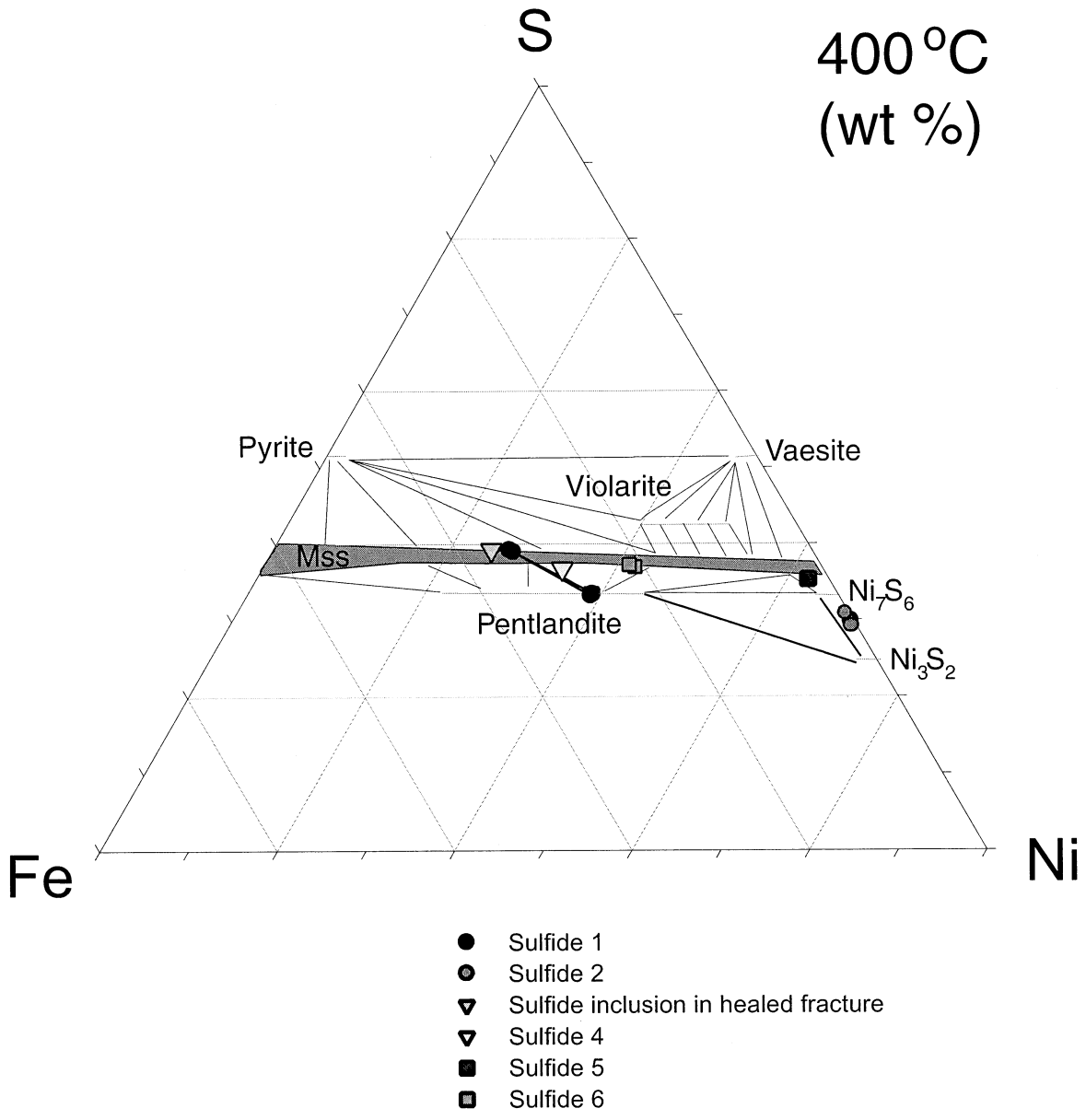

Fig. 3. An isothermal (400°C) section through the "condensed" Fe-Ni-S system (Naldrett, 1989). Data for Fe-Ni sulfides in sample 1026V are plotted here. Chalcopyrite compositions are not included. Each point represents an electron microprobe analysis within a specific sulfide (identified by numbers; see Fig. 2). Tie lines represent coexisting sulfides.

proximately 100 to 200 mg of rock powder were mixed in a Coors crucible with 4 to 6 g of premixed flux, consisting of sodium tetraborate, 99.7% purity 100-200 mesh Ni powder (Alfa-Aesar), and sublimed sulfur powder in the ratio of 20 : 2 : 1, respectively. The ensuing mixture was spiked with a mixed solution of PGE tracers (^{99}Ru, ^{105}Pd, ^{190}Os, ^{191}Ir, ^{198}Pt) and allowed to dry overnight. Rhodium was not measured because it is mono-isotopic. The crucible and its contents were then covered with a ceramic cap and heated at 1050°C for 40 min to 1 h in a muffle furnace. After fusion, the crucibles were taken out of the furnace and allowed to cool in air. This method resulted in the formation of an immiscible Ni-sulfide liquid and a silicate-borate slag. The PGEs in the spike and sample were quantitatively extracted into the sulfide liquid (Re was not extracted into the sulfide bead and therefore a separate aliquot of sample was simultaneously spiked with enriched Re and Os isotopic tracers and then dissolved in sealed glass vessels as described in section 3.3 below). The NiS bead was removed from the crucible, crushed into small pieces, and dissolved in 30 mL of 6.7 N HCl. This resulted in the dissolution of the NiS bead and the precipitation of insoluble PGE-sulfides. After complete dissolution (when H_2S ceased to evolve), the resulting solution was passed through a 0.45-μm cellulose-nitrate filter, which eliminated most of the dissolved Ni. The filtrate was disposed of but the filter paper and its contents (PGE sulfides and any undissolved NiS) were transferred to a 15-mL savillex beaker, into which 0.75 mL of 8 N HNO_3 was added. The beaker was heated at 100°C for 4 h, which resulted in complete (or nearly complete) dissolution of the PGE sulfides and the filter paper. Yield tests indicated at least 80% yield of PGEs during this dissolution process and minor Os loss during heating. Note that loss of PGEs during this step is irrelevant for isotope dilution measurements, because the enriched PGE spike is equilibrated with the sample during the fusion stage. Good reproducibility on an in-house peridotite standard (SC99-1) indicates sample-spike equilibration was achieved (see sec-

tion 3.6 below). One-half of this solution was centrifuged and diluted up to 4 N HNO_3 and was analyzed directly by ICP-MS. The other half of the solution was dried, taken up in 0.15 N HCl, passed through 0.5 mL of cation exchange column (AG50X-8, 100-200 mesh), and run through the ICP-MS. This step removed any remaining Ni from solution, greatly improving Ru measurements by eliminating NiAr interferences (Puchtel and Humayun, 2000).

3.3. Re-Os Isotopic Analyses by Acid Digestion

Re and Os isotopic analyses presented here are reproduced from previously published data (Lee et al., 2000, 2001b; Lee, 2001). In brief, ~1 g of sample powder was placed in a thick-walled borosilicate glass vessel. Reverse aqua regia (two parts concentrated HNO_3 and one part concentrated HCl) and a tracer solution enriched in ^{185}Re and ^{190}Os were added to the vessel, which was then sealed and held at 240°C for 3 d. The closed system nature of this method ensures no volatile loss of Os, while the high temperatures and highly oxidizing nature of aqua regia ensure that the mixed Os and Re tracer equilibrates with the Os and Re in the sample. Re was extracted by anion exchange chemistry, and Os was extracted by carbon tetrachloride solvent extraction, followed by stabilization in 9 N HBr, and finally purified by microdistillation. Os was run by negative thermal ionization mass spectrometry (N-TIMS), and Re was run by ICP-MS. Details of N-TIMS procedures have been described elsewhere (Lee et al., 2000).

3.4. Accuracy of Isotope Dilution Measurements

Single-element enriched tracer solutions were made from enriched isotope powders purchased from Oak Ridge National Laboratory. These were dissolved in aqua regia in sealed, thick-walled borosilicate glass vessels at 240°C. Pt and Pd were dissolved within a few days, but complete dissolution of Ir and Ru took several weeks. Preparation details for the Os spike have been described previously (Lee, 2001; Yin et al., 2001). After dissolution, the resulting solutions were dried down to a small bead and then taken up in 6.7 N HCl.

Accuracy of the enriched isotope solutions was determined by calibrating each single-element enriched isotopic tracer solution against one single-element standard solution with normal isotopic compositions (in 6.7 N HCl) purchased from Johnson Matthey (Specpure Ir, Pt, Pd, Ru) and two gravimetric Os standard solutions prepared from Os salts (Yin et al., 2001). Calibrations were performed by mixing the tracer solutions with standard solutions, followed by direct aspiration (via glass nebulizer and cyclonic spray chamber) into a Micromass multiple-collector ICP-MS (Harvard University). Corrections for mass fractionation were determined by either external calibration (doping with another element, e.g., Pt for Ir, Pd for Ru, and vice versa) or internal corrections using iteration and/or inversion procedures (Lee et al., 2001c; Yin et al., 2001). Johnson Matthey specification sheets indicate that the concentrations of the Re, Ir, Pt, Pd, and Ru normal standard solutions are accurate to within 0.3%. The reproducibilities of the ^{185}Re tracer calibrations are better than the manufacturer's stated accuracy of the Re standard solution. However, reproducibilities (2 standard deviation) of three different spike-normal mixtures made for tracer calibration are Ir = 0.5%, Pd = 2%, Pt = 0.6%, and Ru = 0.9%. Therefore, the accuracies of the Ir, Pt, Pd, and Ru tracer solutions are limited by the calibration uncertainties instead of the manufacturer's stated accuracies of the standard solutions. The accuracy of the ^{190}Os tracer is ~0.3%, based on calibrations against two gravimetric standards (for details, see Yin et al., 2001). A mixed PGE tracer solution (^{190}Pt, ^{191}Ir, ^{105}Pd, ^{99}Ru, ^{190}Os) was created for optimal use with peridotites. A separate ^{185}Re-^{190}Os tracer solution was used for the glass vessel dissolutions. To assess whether the tracer calibrations are biased compared to other laboratories, the mixed PGE tracer solution above was used to determine the PGE contents of well-mixed clay from the Cretaceous-Tertiary boundary at Stevns Klint in Denmark (SK10). The PGE measurements agree to within 10% of measurements made by radiochemical neutron activation analyses in a previous study (Kyte et al., 1985). This sample was chosen as an interlaboratory standard because of its homogeneous character. Limited amounts of SK10 are available on request.

3.5. Mass Spectrometry Details

Analyses of samples were conducted on a magnetic sector, single-collector ICP-MS (Finnigan Element 1). Samples were aspirated into a Scott Spray chamber using a microconcentric nebulizer (Cetac MCN-100). The following masses were analyzed (98, 99, 101, 102, 103, 105, 106, 108, 111, 189, 190, 192, 191, 193, 194, 195, 196, 198, 200) by scanning with the electrostatic analyzer (using two magnet positions). Mass 98 was used to monitor for NiAr interferences on Ru, mass 111 was used for Cd interferences on Pd, and mass 200 was used for interferences on Pt. A blank, consisting of the same acid matrix as the sample, was run before each sample to monitor background. These backgrounds were subtracted from the sample intensities. The PGEs (particularly Os) can leave a significant "memory" in Teflon apparatus and was therefore minimized by using a very short Teflon uptake tube (~10 cm) and allowing enough time for washout (generally, 2 min). Samples were analyzed only if the background had dropped to $< 1\%$ of the sample intensities. These backgrounds were subtracted from the sample intensities. The contribution of Pt^{190} on Os^{190} was negligible. NiAr interferences on Ru^{101} and Ru^{102} were always $< 5\%$. Contribution of Hg^{198} on Pt^{198} was accounted for ($< 10\%$). Mass fractionation was monitored by running a mixed PGE standard at the beginning and end of each run. Mass spectrometry details for Os isotopic analyses determined by thermal ionization mass spectrometry have been described in detail elsewhere (Lee et al., 2000, 2001b; Lee, 2001).

3.6. Procedural Blanks and Reproducibility

Nickel sulfide fire assay procedural blanks (reported as picograms per gram of flux) are reported in Table 1. These procedural blanks are lower than those reported by others (e.g., Puchtel and Humayun, 2000). The Ni powder used here is of lower certified purity (99.7%) than that typically used by others for this type of work (99.99%), but it was observed here to have significantly lower PGE content. External reproducibilities on real samples using the Ni sulfide fire assay technique range from 5 to 10% for the different PGEs, as shown with three repeats (100 to 200 mg fusions) of a well-mixed San Carlos peridotite powder (SC99-1), collected from the San Carlos volcanic field in Arizona (Fig. 4). External reproducibilities on this in-house standard are similar or slightly better than those (3–26%) reported by Puchtel and Humayun (2000) on komatiite standards, having PGE concentrations similar to the peridotites studied here. These reproducibilities indicate tracer-sample equilibration is achieved in our procedure, at least to the level of 5 to 10%. It is not clear if this uncertainty is due to sample heterogeneity.

Procedural blanks for acid digestions using sealed glass vessels are 3 pg for Os and 6 pg for Re (Lee et al., 2000, 2001a,b). Figure 5 compares Os concentrations determined by acid digestion and by fire assay. In general, concentrations agree to within 25% for most samples. However, three Big Creek samples fall significantly outside of the 25% range. One explanation for this is the lack of tracer-sample equilibration. However, given the good reproducibility on the San Carlos in-house standard, this seems unlikely. A more probable explanation is that the Big Creek peridotites are extremely heterogeneous. It is noted that sample 1026V, which has the highest abundance and diversity of sulfides, has the largest discrepancy between the two procedures.

4. RESULTS

Chondrite-normalized (CI-normalized) PGE-Re abundances are shown in Figures 6 , 7, and 8 (normalization values are represented by average of CI chondrites; Anders and Grevesse, 1989). Re and the PGEs are plotted in the following order: Os, Ir, Ru, Pt, Pd, and Re. This ordering scheme was chosen because it gives smooth CI-normalized patterns for komatiites (Puchtel and Humayun, 2000) and is believed to broadly reflect the relative order of compatibility. Re was placed last in the sequence, because it is believed to be the most incompatible of these elements.

The PGE abundances reported here are similar to worldwide averages. The average CI-normalized Ir concentration in this

Table 1.

		Ir ppb Fire Assay ICP-MS	2σm	Os ppb Fire Assay ICP-MS	2σm	Ru ppb Fire Assay ICP-MS	2σm	Pt ppb Fire Assay ICP-MS	2σm	Pd ppb Fire Assay ICP-MS	2σm	Re ppb Carius Tube ICP-MS	Os ppb Carius Tube TI-MS	187Os/188Os Carius Tube TI-MS	Mg/(Mg+Fe) Carius Tube	S ppm
BIG CREEK																
1026V	sp gt lherz	4.1	0.1	8.0	0.3	10.0	0.5	51	5	96	9	0.38	4.41	0.1551	0.910	230
BC77	sp gt harz	3.34	0.05	3.73	0.05	6.9	0.2	5.2	0.1	3.27	0.08	0.30	3.61	0.1263	0.911	32
P10	sp lherz	5.19	0.09	3.79	0.06	7.3	0.1	17.1	0.4	14.3	0.3	0.19	3.87	0.1263	0.909	98
P10*		4.7	0.2	4.2	0.3	7.7	0.5	18	1	9.0	0.6					
P6	sp gt lherz	1.13	0.02	1.00	0.02	2.14	0.05	2.21	0.07	1.85	0.06	0.15	3.39	0.1288	0.902	134
BC98-2	sp harz	4.6	0.1	4.0	0.1	5.8	0.2	5.6	0.3	3.0	0.2	0.09	4.31	0.1219	0.913	
P7	sp lherz	3.7	0.1	3.7	0.1	6.3	0.3	7.7	0.5	10.4	0.5	0.19	4.00	0.1296	0.901	143
P1	sp lherz	4.8	0.1	5.6	0.2	7.0	0.4	9.8	0.5	6.6	0.3	0.25	3.65	0.1279	0.886	
BC98-1	garnet websterite	0.078	0.005	0.04	0.01	0.16	0.01	1.8	0.1	1.13	0.05	0.60	0.06	0.3453		
OAK CREEK																
OK98-3	sp lherz	4.45	0.08	1.35	0.03	7.2	0.3	9.1	0.3	2.5	0.1	0.053	1.14	0.1309	0.895	26
OK98-4	sp lherz	4.2	0.2	1.34	0.08	7.4	0.6	8.4	0.4	2.5	0.2	0.12	1.53	0.1271	0.894	67
OK98-2	sp lherz	3.61	0.09	2.8	0.1	6.4	0.4	4.5	0.2	2.2	0.1	0.080	2.84	0.1235	0.896	
CIMA																
CiP98-64	sp harz	3.19	0.05	1.31	0.04	8.4	0.2	5.9	0.1	4.9	0.1	0.074	1.65	0.1225	0.908	24
Ki5-16	sp harz	3.81	0.06	2.08	0.02	4.52	0.05	2.10	0.04	0.79	0.01	0.030	1.35	0.1120	0.911	20
Ki5-139	pl sp lherz	3.07	0.03	1.29	0.02	4.5	0.1	4.23	0.07	2.9	0.2	0.073	1.30	0.1288	0.893	85
Ki5-32	sp harz	4.14	0.04	2.69	0.03	8.3	0.2	5.5	0.1	2.59	0.06	0.14	2.03	0.1228	0.906	33
SAN CARLOS																
SC99-1-a	sp lherz	3.68	0.06	1.20	0.03	6.3	0.2	6.0	0.2	2.42	0.07					30
SC99-1-b		3.1	0.1	1.43	0.04	5.8	0.3	6.2	0.3	2.28	0.07					
SC99-1-c		3.32	0.05	1.23	0.02	5.5	0.1	5.6	0.1	2.21	0.05					
ave		3.4		1.3		5.9		5.9		2.3						
1 R. S. D.		0.09		0.10		0.06		0.05		0.05						
PROCEDURAL BLANKS		pg/g of flux		pg/g of flux		pg/g of flux		pg/g of flux		pg/g of flux						
BL901		0.6		0.3		4		5		41						
BL91801		0.7		0.1		5		5		23						
ave		0.6		0.2		4		5		32						
1 R. S. D.		0.09		0.65		0.16		0.001		0.39						

sp = spinel; gt = garnet; lherz = lherzolite; harz = harzburgite; ave = average; R. S. D. = relative standard deviation; 2σm = 2 standard deviation of the mean; ICP-MS = inductively coupled plasma mass spectrometry; TI-MS = thermal ionization mass spectrometry.

study is 7.88×10^{-3} (3.79 ppb) (cf. a worldwide average of $(6.7 \pm 0.5) \times 10^{-3}$ (3.22 ppb) reported by Morgan et al., 2001). Sulfur concentrations (20–230 ppm) are also similar to worldwide averages of peridotites; xenoliths typically have < 50-ppm S and unaltered massif peridotites have < 300-ppm S (Lorand, 1989). There appears to be no correlation between absolute PGE and S content. When the data are viewed as a whole, the Os/Ir ratios appear to be roughly correlated with S content (Fig. 9a), but the correlation breaks down if each xenolith suite is viewed separately.

4.1. Big Creek

4.1.1. Peridotites

There appears to be regional coherence in PGE-Re relative abundance patterns. With the exception of sample 1026V, Big Creek peridotites show slightly negative to slightly positively sloped PGE-Re patterns (Fig. 6a), the latter associated with superchondritic Pd/Ir in three samples (average Pd/Ir = 1.7 ± 0.8, excluding sample 1026V, which has Pd/Ir = 23.5). The two samples with the highest Mg#s are depleted in Pt and Pd relative to Ir and Ru. All Big Creek samples have near-chondritic Os/Ir and subchondritic to chondritic Re/Os ratios, with the exception of sample 1026V, which has distinctly superchondritic Os/Ir and subchondritic Re/Os. These Big Creek peridotites have PGE-Re patterns similar to lherzolites (chondritic signature) and harzburgites (depletions in Pt and Pd) from Pyrenean orogenic ultramafics (Lorand et al., 1999).

4.1.2. Garnet websterite (BC98-1)

The garnet websterite (BC98-1) has extremely low PGE abundances and shows a very steep, positive relative abundance pattern (Fig. 6a). The PGE signature of BC98-1 closely matches that of some primitive basalts (Puchtel and Humayun, 2001).

4.1.3. Peridotite 1026V

Although similar to the other Big Creek peridotites in terms of major elements and silicate petrography (Lee et al., 2001a), sample 1026V from Big Creek is anomalous because it has abundantly visible sulfides (including the presence of chalcopyrite; Figs. 2, 3), high S, Pd, Pt, and Os contents and a high $^{187}Os/^{188}Os$ ratio (Figs. 6c, 7, 8, 9, 10). The enrichment in Os, Pt, and Pd relative to Ru and Ir seen in sample 1026V (Figs. 6, 7, 8, 9) is reminiscent of some spinel and plagioclase lherzolites

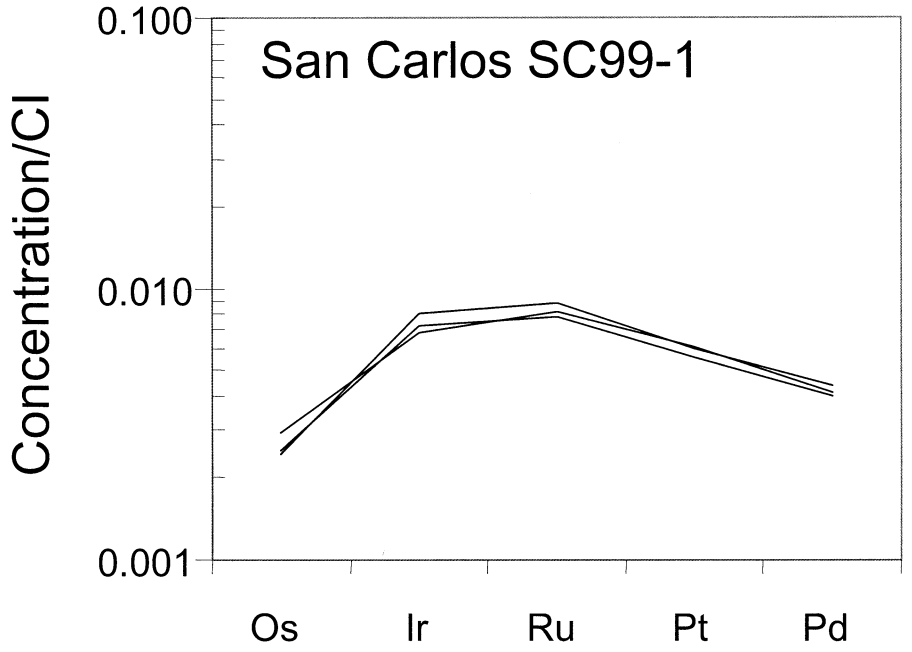

Fig. 4. Chondrite-normalized (CI) PGE abundances determined by nickel-sulfide fire assay on an in-house reproducibility standard (San Carlos SC99-1). Chondrite (CI) values are taken from Anders and Grevesse (1989).

from the Lanzo peridotite massif in Italy (Lorand et al., 2000). It is also unusual that the Os concentration determined by glass vessel dissolution is much lower than that determined by the fire assay technique (Fig. 5; Table 1). This is interpreted to reflect extreme sample heterogeneity associated with the nugget effect of the sulfides and the coarse-grained nature of the sample.

4.2. Oak Creek

Oak Creek peridotites show convex PGE abundance patterns due to depletions in Os, Pt, Pd, and Re relative to Ir and Ru (Fig. 6b). The average Pd/Ir is 0.6 ± 0.1. The depletion in Os relative to Ir is commonly observed in mantle xenolith samples

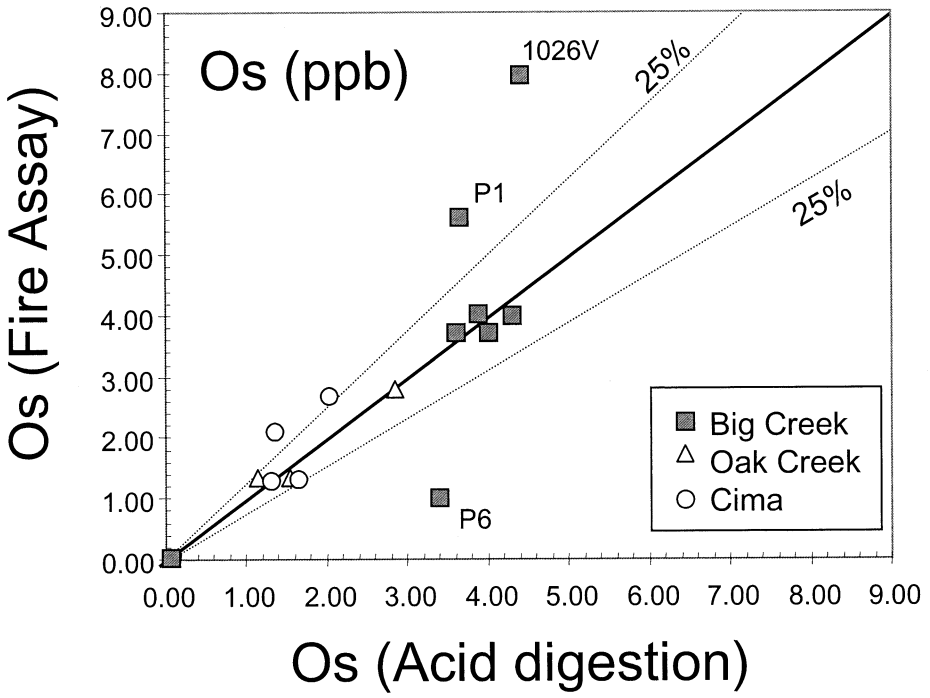

Fig. 5. Comparison of Os concentrations (ppb) by acid digestion (in sealed glass vessels) and nickel-sulfide fire assay. Solid line represents 1 : 1 line.

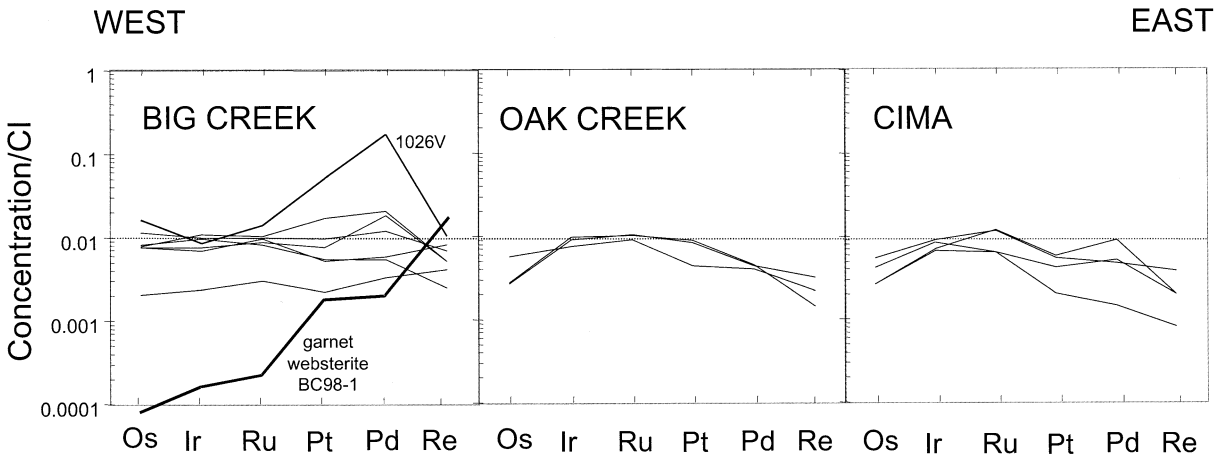

Fig. 6. CI-normalized abundances of all peridotite samples measured in this study. BC98-1 (thick line) represents a garnet websterite. All PGE abundances (including Os) refer to nickel-sulfide fire assay numbers, while Re numbers reflect acid digestion techniques.

(Handler et al., 1999). Although the relative depletions in Pt and Pd are similar to some orogenic harzburgites (Lorand et al., 1999), the Oak Creek peridotites are fertile lherzolites (Mg# ~0.89).

4.3. Cima

Cima peridotites are also depleted in Os relative to Ir (Fig. 9a) but have near-chondritic to subchondritic Pt/Ir, Pd/Ir, and Re/Os (Fig. 6c). Average Pd/Ir is 0.8 ± 0.5. Despite the large variations in Pd/Ir and Os/Ir, the Ru/Ir ratios remain broadly chondritic. The lowest Pd/Ir is represented by the most refractory sample, Ki5-16 (Mg# = 0.911). It is noteworthy that the absolute and relative PGE abundances in the Cima peridotites differ from peridotites from the nearby Dish Hill cinder cone (Wilson et al., 1996). Wilson et al. (1996) report average Ir concentrations of 0.6 ppb and flat PGE abundance patterns, contrasting with an average of 3.55-ppb Ir and flat to negatively sloped PGE patterns in the Cima peridotites.

4.4. Re-Os Isotopic Systematics

Re-Os isotopic systematics have already been reported and discussed in Lee et al. (2000, 2001b) but are shown here for completeness (Table 1; Fig. 10). In brief, the majority of the Big Creek and Oak Creek peridotites analyzed here for PGE abundances have $^{187}Os/^{188}Os$ ratios similar to estimates of "primitive" upper mantle (Meisel et al., 1996). The exception is sample 1026V, which has a very radiogenic $^{187}Os/^{188}Os$ ratio (0.1551), which is not supported by its Re abundance (Fig. 10a). There is one Big Creek sample, i.e., P2 in Lee et al. (2000), with very unradiogenic $^{187}Os/^{188}Os$ (0.1163), which was not included in this study because there was no more sample available for analysis. This sample has an Re-depletion model age of ~1.7 Ga (Lee et al., 2000), assuming a present-day "primitive" upper mantle composition of ~0.1296 (Meisel et al., 1996). Cima peridotites are distinctly unradiogenic (Fig. 10a), giving Re-depletion model ages up to 2.4 Ga (sample Ki5-16). Taken at face value, these data indicate that the Re/Os ratios of the Big Creek and Oak Creek peridotites were fractionated recently (Phanerozoic), while those for Cima peridotites reflect ancient (late Archean to early Proterozoic) fractionation (Lee et al., 2000, 2001b).

5. DISCUSSION

5.1. Depletions in Pt, Pd, Re, and Os Relative to Ru and Ir

In Figure 7, constant Ru and Ir concentrations and near-chondritic Ru/Ir ratios (within 25%) over a wide range in fertility (Mg# = 0.89–0.91) suggest that Ru and Ir are both compatible during partial melting. However, one sample (Ki5-16), characterized by strong depletions in Pt and Pd relative to Ir, has a low Ru/Ir ratio (1.18; cf. CI Ru/Ir = 1.48). If Ir is indeed strongly compatible and if a chondritic initial composition is assumed, it follows that the subchondritic Pt/Ir, Pd/Ir, Os/Ir, and Re/Ir ratios in the Oak Creek and Cima peridotites reflect lower compatibilities of Pt, Pd, Os, and Re relative to Ir (in order of decreasing compatibility). In this context, the slightly superchondritic Pt/Ir and Pd/Ir ratios in some of the Big Creek peridotites and the extremely superchondritic Os/Ir, Pt/Ir, and Pd/Ir ratios seen in the anomalous Big Creek sample 1026V reflect secondary enrichments. This section addresses the possible origins of depletions in Pt, Pd, Os, and Re relative to Ru and Ir.

If it is first assumed that all of the depletions in Pt, Pd, Os, and Re are related to partial melting, then a straightforward interpretation of the relative magnitudes of these depletions is that their bulk peridotite/melt partition coefficients (D) are less than those for Ru and Ir. The order of decreasing compatibility should then follow $D_{Ir} \sim D_{Ru} > D_{Pt} > D_{Pd} \sim D_{Os} > D_{Re}$. To explain the magnitude of some of the Pt, Pd, Os, and Re depletions (40–50% depletion in Pt, Pd, Os and/or Re relative to chondritic Ir proportions; Fig. 7b, 8b), these elements must be moderately incompatible during melting, e.g., $D < 1$. This becomes clear by considering a simple calculation. Assuming

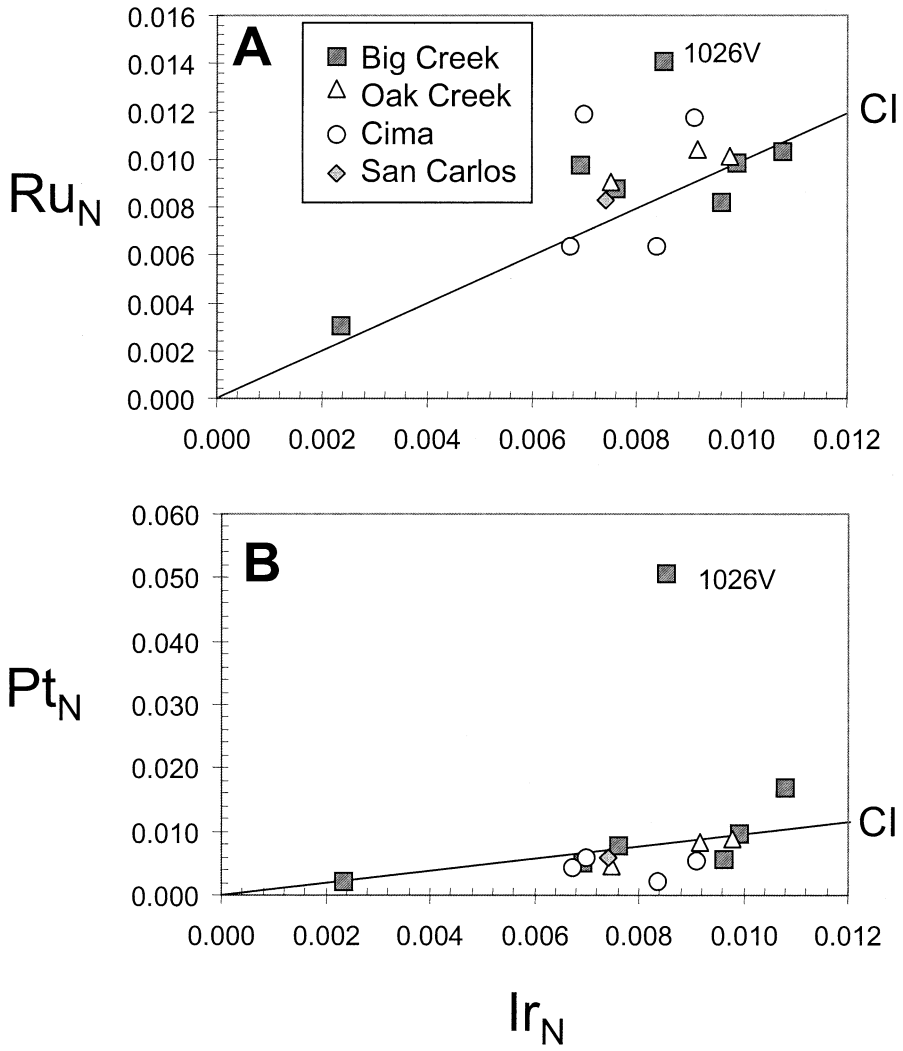

Fig. 7. CI-normalized plots of Ru and Pt vs. Ir. Line represents the chondritic reference line.

fractional melting, the fractionation of an element relative to Ir in the residue is given by

$$(C_i/C_{Ir})/(C_i^o/C_{Ir}^o) = (1 - F)^{1/D_i - 1/D_{Ir}}$$

where C_i and C_{Ir} are the concentrations of element $_i$ and Ir in the residue, C_i^o and C_{Ir} are the initial concentrations of element i and Ir, D_i and D_{Ir} are the bulk solid/melt partition coefficients, and F is the mass fraction of melt extracted. From this equation, it can be seen that if Pd and Ir are both compatible, the value of the exponent will be a small number, and hence the Pd/Ir ratio will be difficult to fractionate by partial melting. For example, if D_{Ir} is assumed to be strongly compatible ($\sim$20), it can be deduced from the above equation that D_{Pd} must be < 1 to decrease the Pd/Ir ratio of the residue to $\sim$50% of its initial value for 20% fractional melting. If D_{Pd} is $\sim$1, the Pd/Ir ratio drops to only 80% of its initial value. If the initial relative abundances of PGEs and Re are chondritic, and if the depletions are all attributed to partial melting effects, it follows that any large depletions in Pt, Pd, Os, and Re relative to Ir (e.g., in the Cima peridotites) require incompatible behavior or secondary loss.

It is likely, however, that the mechanisms for depletion of Pt, Pd, Os, and Re are much more complex than implied by the above discussion. In particular, the possibility for decoupled PGE-Re behavior needs to be addressed. These complexities are described as follows: The order of PGE-Re enrichment seen in primitive mantle-derived melts (from depleted to enriched, these are Os, Ir, Ru, Pt, Pd, and Re) qualitatively reflects the order of effective bulk incompatibility during partial melting. The depletions in Pt, Pd, and Re in the California peridotites indeed mirror the enrichments in Pt, Pd, and Re in primary mantle melts and are hence consistent with the order of compatibility inferred from melt compositions. However, the depletions in Os in the Oak Creek and Cima peridotites do not have a complementary enrichment in primitive silicate melts (Barnes et al., 1985; Puchtel and Humayun, 2001). In addition, depletions in Pd/Ir appear not to be correlated with major-element indices for the degree of melting, such as Mg#. For example, even though the largest depletions in Pd and Re

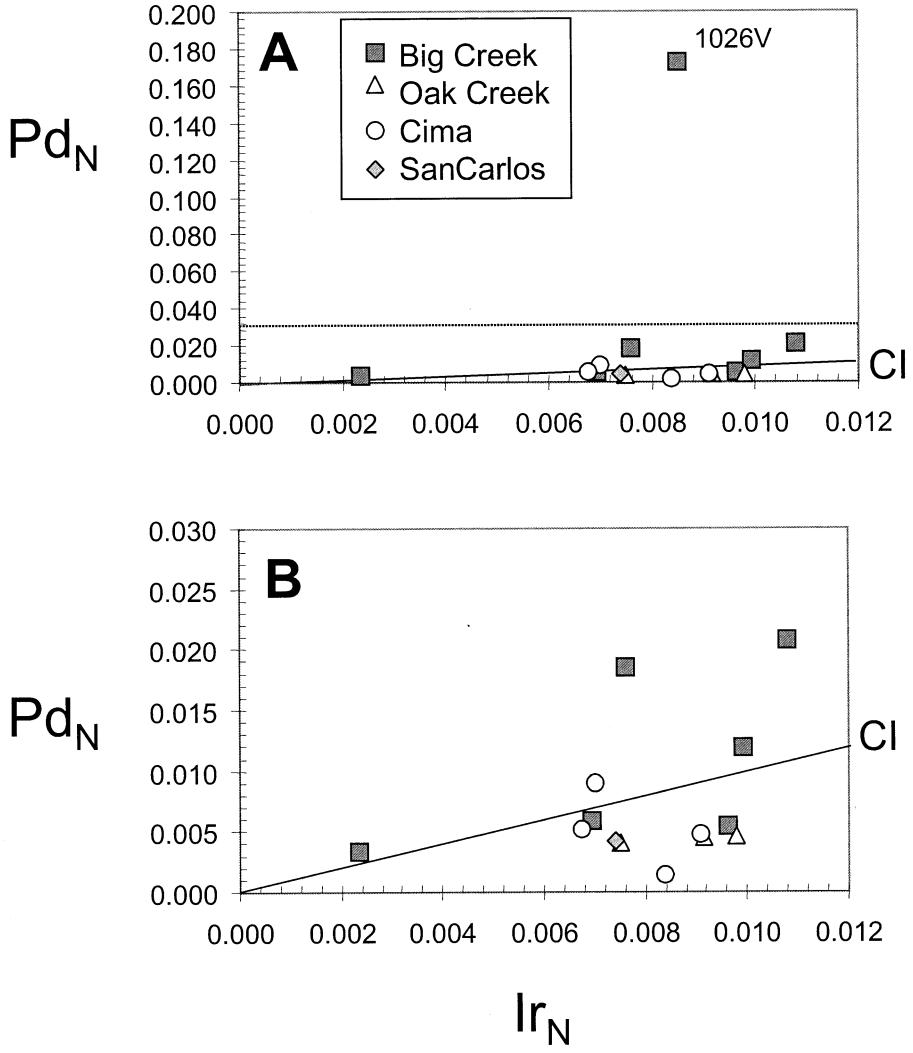

Fig. 8. CI-normalized plots of Pd vs. Ir. Bottom panel is a blowup of the outlined region in the top panel. Line represents chondritic reference line.

relative to Ir are seen in the most refractory samples (e.g., Cima Ki5-16), Big Creek peridotites (excluding 1026V) have slightly subchondritic to slightly superchondritic Pd/Ir ratios, although their Mg# numbers are quite high (Fig. 6a; Table 1). In contrast, Oak Creek peridotites have subchondritic Pd/Ir ratios (Fig. 6b), even though they are relatively fertile in terms of major elements. Os depletion also appears to be decoupled from major-element indices as illustrated by chondritic Os/Ir ratios in the refractory Big Creek peridotites (with the exception of 1026V) but distinctly subchondritic ratios in the fertile Oak Creek peridotites. It is thus clear that the depletions in Pt, Pd, Os, and Re relative to Ir in these Californian xenoliths are not always correlated with major-element indices of the degree of melting as has been seen in some massif peridotites.

Below, I discuss possible means of depleting Pt, Pd, Os, and Re with respect to Ru and Ir. Enrichment mechanisms are treated in section 5.2. In brief, it will be shown that it is probably not possible to explain all of the depletions in Pt, Pd, Os, and Re by any single mechanism. In addition, it will also be realized that further progress on understanding the partitioning of PGEs and Re in peridotites requires detailed petrographic analyses of minor and trace phases, such as chromites, sulfides, and platinum group minerals. This level of detailed petrographic analysis was not conducted in this study.

5.1.1. Sulfides

It is well known that PGEs and Re are highly compatible in sulfides relative to silicate melts. The sulfide/silicate melt partition coefficients of Pt, Pd, Ru, Ir, and Os are all very large ($\sim 3 \times 10^4$) and nearly identical (Fleet et al., 1991; Crocket et al., 1992, 1997; Peach et al., 1994). The sulfide/silicate melt partition coefficient for Re is also very large, ranging from 10 to 10^3 (Jones and Drake, 1986; Roy-Barman et al., 1998). It is thus reasonable to postulate that partitioning of PGE-Re during partial melting may be largely controlled by the presence of sulfide in the residue. For example, using a sulfide/silicate melt partition coefficient for Ir of $\sim 3 \times 10^4$ and assuming that the amount of sulfide in a fertile peridotite is ~0.07 wt.% (assuming fertile peridotite has ~250 ppm S), the bulk peridotite/

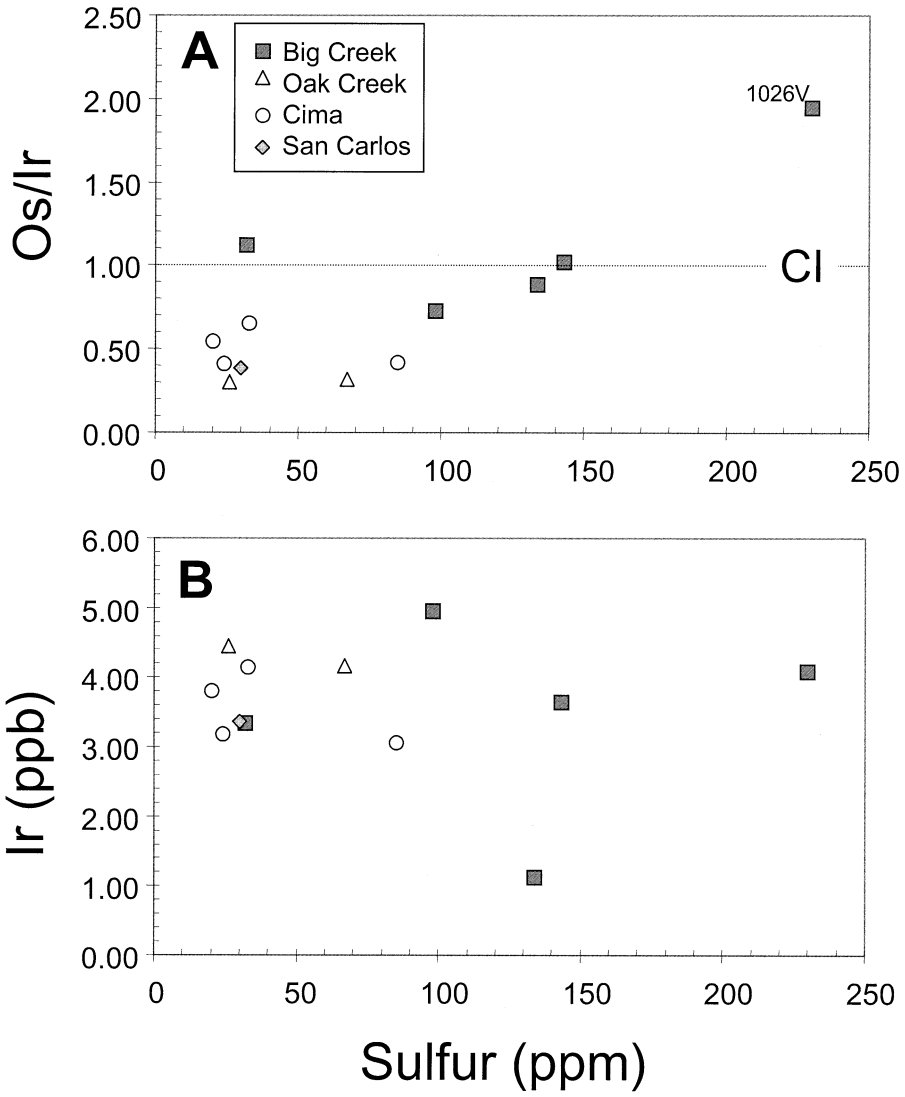

Fig. 9. (A) Os/Ir vs. S concentration (ppm). Dotted line is the chondritic Os/Ir value. (B) Ir (ppb) vs. S (ppm).

silicate melt partition coefficient will be ~20, hence highly compatible. Handler and Bennett (1999) were able to model the rough positive correlation between PGE content and S content in peridotite xenoliths from southeast Australia by the progressive depletion of sulfide.

As demonstrated above, however, it is practically impossible to significantly fractionate relative abundances of elements that have high and nearly identical compatibilities. One way to bypass this difficulty is to invoke partitioning of PGEs between monosulfide solid solution (mss) and sulfide (sf) melt (Fleet et al., 1993). Fleet et al. (1993) showed that Pt and Pd are incompatible in the monosulfide solid solution ($D^{mss/sf\ liq} < 0.2$), while Os, Ir, and Ru are compatible ($D^{mss/sf\ liq} = 3–5$). This provides a means of fractionating Pt and Pd (but not Os) from Ir and Ru. However, this scenario is still not entirely satisfactory in explaining the PGE-Re systematics of the California xenoliths in the present study. Figure 9b shows that Ir contents are constant over a wide range in S compositions, ranging from 10- to 250-ppm S. Assuming that S content is directly correlated with sulfide content in these peridotites, it must be concluded that Ir contents (and by inference, Ru contents) are not strongly correlated with sulfide abundance. This suggests that partitioning of Ru and Ir in peridotites may not be entirely controlled by sulfides.

5.1.2. Alloys and spinels

If interstitial sulfides are exhausted or absent, then the question arises, What controls the partitioning of PGEs and Re? Experimental studies suggest that Ru may be compatible in chromian spinel but Pd is incompatible (Capobianco and Drake, 1990; Capobianco et al., 1994). However, field observations suggest that Ru and Ir are excluded from chromian spinel (Maier and Barnes, 1999; Maier et al., 1999). In addition, many detailed petrographic studies have documented the presence of platinum group element minerals (PGMs) hosted as inclusions in chromian spinels from layered intrusions (e.g., Maier et al., 1999, and references therein). The most abundant

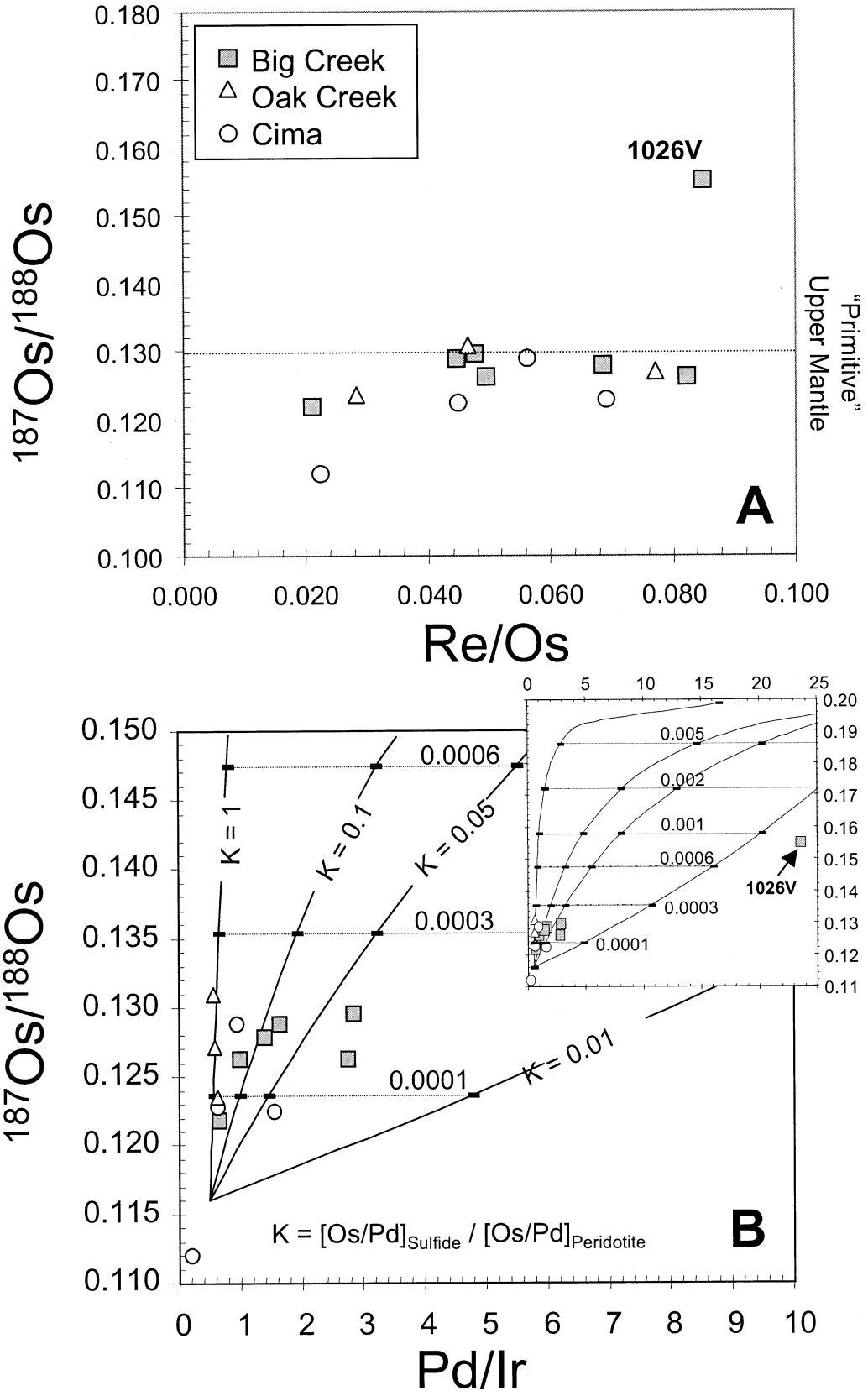

Fig. 10. (A) $^{187}Os/^{188}Os$ vs. Re/Os ratio. (B) $^{187}Os/^{188}Os$ vs. Pd/Ir ratio. Curves are mixing lines representing the addition of radiogenic sulfides to a peridotite with a Pd/Ir ratio of 0.5 and a $^{187}Os/^{188}Os$ ratio of 0.116, the least radiogenic Sierran peridotite observed by Lee et al. (2000). The radiogenic sulfide was chosen to have a Pd/Ir ratio of 30 (approximately matching 1026V's Pd/Ir), a $^{187}Os/^{188}Os$ ratio of 0.2, and a range of Pd/Os ratios, ranging from K = 0.01 to 1 ($K = [Os/Pd]_{Sulfide}/[Os/Pd]_{Peridotite}$). The weight fractions of the radiogenic sulfide added to the peridotite are denoted as tick marks and connected by dotted lines. For reference, the approximate weight fraction of sulfide in a typical peridotite is $<$ 0.0007, assuming fertile peridotites have ~250-ppm S (Lorand, 1990) and sulfides have ~350,000 ppm S.

PGMs in ophiolites appear to be laurite [$(Ru,Os,Ir)S_2$] and rutheniridosmine (Ru-Ir-Os alloy), while Pt-, Pd-, and Rh-bearing PGMs are quite rare (Legendere and Auge, 1986). Finally, experimental studies have confirmed that Ru-Os-Ir alloys are stable at chromian spinel-based liquidus temperatures, indicating that PGM inclusions in chromian spinels are probably primary magmatic features (Brenan and Andrews, 2001). These studies suggest that alloy phases included in chromian spinels may be responsible for the apparent compatibility of Os, Ru, and Ir in chromian spinels, providing a means of decoupling Pt and Pd from Os, Ir, and Ru. In this context, we note that (1) Ir concentrations are constant over a wide range of sulfur contents if all of the data are examined together, and (2) Pt and Pd depletions appear to be greatest in the Oak Creek and Cima peridotites, which are characterized by low S abundance and a general lack of visible sulfide. Although clearly speculation, the observed PGE abundances can be reconciled if (a) Pt and Pd are controlled by sulfide and hence become incompatible when sulfide is exhausted or depleted, and (b) Os, Ru, and Ir are retained strongly in spinels or alloys. This scenario cannot easily explain the decoupling of Os from Ru and Ir if Os is considered to have similar behavior as Ru and Ir.

5.1.3. Aqueous fluids

One mechanism for fractionating Os and Pd from Ir during melting is to invoke the presence of high-temperature aqueous fluids. Os and Pd may be mobilized in such fluids, because the former may be volatile as an oxide and the latter volatile as a chloride complex in high-temperature fluids (Wood, 1987). In contrast, Ir appears to be less mobile in such fluids (Wood, 1987). This provides a means of decoupling Os from Ir, which neither sulfides nor alloys can accomplish. If the peridotites experienced a one-stage melting history (and no enrichments), then a simple interpretation in the current context is that the chondritic Os/Ir and Pd/Ir ratios seen in the Big Creek peridotites imply melting in a fluid-free environment, and the subchondritic Os/Ir and Pd/Ir ratios in the Oak Creek and Cima peridotites imply melting in the presence of fluids. Such an interpretation, however, comes as a surprise, because Big Creek is closer to the arc front than Cima (Fig. 1), and, therefore, Big Creek would be expected to have experienced more fluid fluxing than Cima. In sections 5.2.2 and 5.2.3 below, we will examine the role of aqueous fluids in causing enrichments in Os and Pd.

5.1.4. Secondary processes

I now explore the possibility that the low Os and S contents of some of these xenolithic peridotites are related to secondary processes unrelated to partial melting, e.g., loss during eruption, emplacement, or weathering. Handler et al. (1999) proposed that the subchondritic Os/Ir ratio of many xenolithic peridotites was due to loss of Os (and retention of Ir) during secondary breakdown of sulfides, perhaps during the decompression associated with eruption (although the actual mechanism for Os loss and Ir retention during this hypothetical process has not been identified). They noted that Os depletion relative to Ir is a common feature of xenoliths and is roughly correlated with anomalously low S contents, compared to orogenic peridotites, which have higher S and Os contents (Lorand, 1990). If the xenolith data in Figure 9a are viewed as a whole, there appears to be a rough correlation between Os/Ir ratio and S content, which is consistent with this interpretation. However, when each xenolith suite is examined separately, the correlations break down. In addition, except for the metasomatized sample 1026V, no obvious products of sulfide breakdown, such as Fe-oxides or -oxyhydroxides, were observed in any of the xenoliths. It is clear that a more detailed study is needed to test the sulfide breakdown hypothesis and to assess whether such a process can also cause depletions in other PGEs (e.g., Pd) relative to Ir.

5.2. Pd and Os Enrichments

5.2.1. COPPS metasomatism

Big Creek sample 1026V deserves special discussion because of its highly anomalous character in terms of high S, Pd, Pt, and Os contents and high $^{187}Os/^{188}Os$ ratio (Figs. 6a, 8, 9a, 10). Coincident with the high S content is the fact that this is the only Big Creek sample with visible sulfides. In addition, chalcopyrite is fairly common in 1026V (Figs. 2, 3). It is thus clear that this sample has experienced secondary addition of sulfides, Cu, Pt, Pd, and radiogenic Os. Although this sample is highly anomalous, a detailed discussion follows, because it is intellectually interesting. For simplicity and sanity, the following discussion assumes that all of these enrichments are related; hence, this sort of metasomatism is termed "COPPS (copper, osmium, platinum, palladium, sulfide) metasomatism." Two questions arise: What is the mechanism and origin of COPPS metasomatism? What effect did this metasomatism have on the other xenoliths?

5.2.2. COPPS transport media

The enrichment in Cu, Pt, and Pd in this metasomatic agent is consistent with the composition of mantle melts. Puchtel and Humayun (2000, 2001) showed that Cu, Pt, and Pd are highly enriched in komatiites (sulfide undersaturated), indicating that Cu, Pt, and Pd are incompatible in fractionating phases such as chromite and olivine. Sulfides that eventually crystallize from such magmas after they have cooled will inherit this signature. Luguet et al. (2001) reported in situ analyses of peridotitic sulfides (laser ablation ICP-MS) and showed that not only is Pd highly enriched in sulfides, but it is also considerably enriched in chalcopyrites ($>$ 100 ppm), which may be of metasomatic origin. These observations suggest that sulfides derived from silicate melts may be a medium for coupled enrichment of Pt, Pd, and Cu. However, simultaneous enrichment in Os is not predicted by these studies: Komatiites have near-chondritic Os/Ir ratios (Puchtel and Humayun, 2000) and chalcopyrites have not been reported to have high Os contents (Luguet et al., 2001). This implies that the enrichment in Os is unrelated to the enrichments in Cu, Pt, Pd, and S, or that the relationship between all of these elements is much more complex.

However, there is circumstantial evidence that the COPPS association may indeed reflect a single style of PGE metasomatism rather than the accumulated effects of several independent events. Mantle xenoliths from the Lihir arc have bulk compositions suggesting coupled enrichment in Cu, Pt, Pd, Os,

and S (McInnes et al., 1999), which is consistent with the COPPS association seen in 1026V. In addition, recent experiments have shown that Cu, Ni, and Pt transport is enhanced in sulfurous fluids (Baker et al., 2001), although Os and Pd transport was not considered in this study. The transport of Os and Pd in aqueous fluids, however, was considered by Wood (1987), using thermodynamic calculations. He showed that OsO_4 and Pd-chloride complexes are highly volatile in aqueous fluids and, therefore, could be transported by and concentrated in metasomatic fluids. Such processes have been inferred to affect Os isotope systematics in arc peridotites (Brandon et al., 1996, 1999; McInnes et al., 1999; Peslier et al., 2000).

5.2.3. Protolith of radiogenic Os in COPPS

An important observation to recognize is that the COPPS metasomatic agent is enriched in Os and is very radiogenic ($^{187}Os/^{188}Os = 0.1551$, compared with 0.1163–0.1310 for the other Sierran xenoliths), but its radiogenic signature is not supported by the rock's low Re/Os ratio (Fig. 6a). This requires more Os than Re to be mobilized into the metasomatic agent, but it paradoxically requires the source of the metasomatic agent to be characterized by high time-integrated Re/Os to generate the very radiogenic Os signature. This behavior is opposite to the more typical behavior of Os being compatible and Re being incompatible. Garnet websterites interleaved at depth with peridotites (Lee et al., 2001a) may be a possible source, because partial melting of this garnet-rich source might allow Re to be sequestered in the residue due to Re's compatibility in garnet, provided sulfide is absent (Righter and Hauri, 1998). The Re/Os ratio of the garnet websterite (BC98-1) is ~10, far higher than the chondritic ratio of ~0.4. However, BC98-1 has extremely low Os (40–60 ppt) contents (Fig. 6a; Table 1). Partial melts of such a lithology will therefore have very low Os contents, and it follows that the Os in the metasomatic sulfide must be concentrated from considerable amounts of garnet websterite to have enriched 1026V in Os. To illustrate: If ~1 ng/g of the Os in 1026V originates from the garnet websterite, then for every gram of unmetasomatized peridotite, Os from at least 250 g of garnet websterite must be quantitatively added to the peridotite in the form of sulfide. If the amount of metasomatic Os in 1026V is more than 1 ng/g, and/or if Os is not quantitatively extracted into the melt from the garnet websterite, then much more garnet websterite must be processed to attain the necessary amount of metasomatic Os. It is not clear if these requirements are physically plausible. If the metasomatic Os was instead derived from an aqueous fluid, a similar calculation can be done to estimate the minimum aqueous fluid/rock ratio, if the concentration of Os in an aqueous fluid were known. The concentration of Os in high-temperature fluids is unfortunately not known. The origin of COPPS metasomatism in 1026V thus remains uncertain.

5.2.4. Effects of COPPS metasomatism on other xenoliths

The $^{187}Os/^{188}Os$ ratios of the Sierran peridotites (except for sample 1026V) were interpreted by Lee et al. (2000) as being primary, and thus they interpreted the "primitive mantle"-like Os isotopic compositions to reflect recent derivation from the asthenospheric mantle. In light of the evidence for radiogenic Os metasomatism in 1026V, the possibility of metasomatic overprinting of Os in the remaining xenoliths deserves attention. The question is whether the Sierran peridotites were originally less radiogenic and have subsequently had their Os isotopic compositions raised by the COPPS metasomatism seen in 1026V.

Figure 10b shows the effect of adding radiogenic sulfides to a peridotite with a Pd/Ir ratio of 0.5 and a $^{187}Os/^{188}Os$ ratio of 0.1163 (the least-radiogenic Sierran peridotite observed by Lee et al., 2000). The radiogenic sulfide was chosen to have a Pd/Ir ratio of 30 (approximately matching 1026V's Pd/Ir ratio), a $^{187}Os/^{188}Os$ ratio of 0.2, and a range of Pd/Os ratios, ranging from K = 0.01 to 1 ($K = [Os/Pd]_{Sulfide}/[Os/Pd]_{Peridotite}$). The $^{187}Os/^{188}Os$ ratio of the hypothetical radiogenic sulfide endmember was chosen somewhat arbitrarily, because the identity of the source is unknown; nevertheless, this endmember composition lies between that of the metasomatized sample 1026V and the garnet websterite BC98-1. The weight fractions of the radiogenic sulfide added to the peridotite are denoted as tick marks. For reference, the approximate weight fraction of sulfide in a typical peridotite is < 0.07 wt.%, assuming fertile peridotites have ~250-ppm S (Lorand, 1990) and sulfides have ~350,000-ppm S.

It is clear from these calculations that the $^{187}Os/^{188}Os$ of some of the Sierran peridotites can be explained by the addition of radiogenic sulfide. However, such an interpretation is too simplistic. The fact that the data as a whole do not fall on any particular mixing line requires the addition of sulfides with very diverse Pd, Ir, and Os contents. For the parameters used in Figure 10b, the values of $[Os/Pd]_{Sulfide}/[Os/Pd]_{Peridotite}$ required to explain the data would range from 0.04 to 1. However, this is a minimum estimate of the range of possible sulfide compositions, because the calculations assume that the Pd/Ir and $^{187}Os/^{188}Os$ ratios of the metasomatic sulfides are fixed, which is probably not the case in nature. Given that primary mantle sulfides exhibit considerable variation in PGE contents (Alard et al., 2000; Luguet et al., 2001) and the likelihood that metasomatic sulfides will show even more variation, it seems highly fortuitous that the addition of a diversity of radiogenic sulfides to a peridotite would result in such homogeneous $^{187}Os/^{188}Os$ ratios. In addition, values of K ~1 seem highly unlikely, because a metasomatic sulfide is likely to be much more enriched in Pd than a typical primary peridotitic sulfide. For example, although the compositions of the sulfides were not measured directly in 1026V, it is reasonable to infer that the sulfides associated with sample 1026V's highly enriched Pd contents are similarly enriched in Pd. It follows that the Oak Creek samples, and at least some of the Big Creek samples, which fall close to the K = 1 mixing line, could not have experienced significant PGE metasomatism. The singular nature of sample 1026V is thus highlighted by its extremely anomalous $^{187}Os/^{188}Os$ and PGE abundance pattern (Fig. 10a and inset in Fig. 10b). It is thus unlikely that the Os isotopic compositions in the majority of the Sierran peridotites reflect PGE metasomatism in the form of the COPPS association. Although the superchondritic Pd/Ir ratios in some of the Big Creek samples must indeed be due to secondary enrichments in Pd, the homogeneity of $^{187}Os/^{188}Os$ argues that such enrichments did not significantly change the $^{187}Os/^{188}Os$ of the bulk rock.

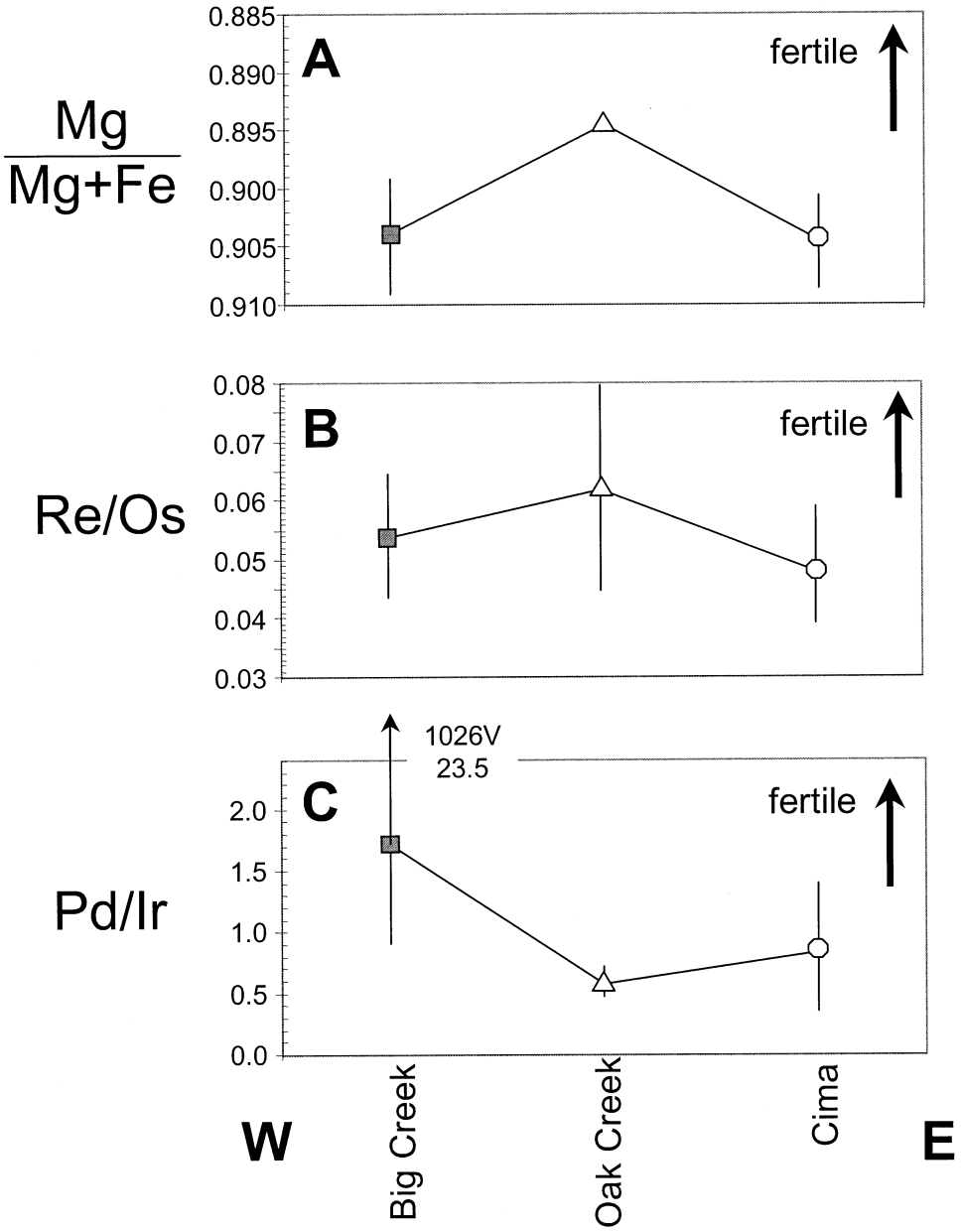

Fig. 11. Regional variations of various geochemical indices. (A) Average Mg/(Mg+Fe). The axis has been reversed so that more fertile samples plot upwards (lower Mg/(Mg+Fe)). (B) Average Re/Os. (C) Average Pd/Ir. The highly anomalous peridotite, 1026V, and the garnet websterite, BC98-1, are excluded from the averages because of their anomalous Pd/Ir ratios. Error bars represent one standard deviation.

5.3. Regional Variations

Figures 6 and 11 show that there may be subtle differences in the PGE-Re abundance patterns among the xenolith localities: Big Creek has the highest average Os/Ir and Pd/Ir ratios, while Oak Creek and Cima have the lowest Os/Ir and Pd/Ir. It is important to note that these differences in Os/Ir and Pd/Ir also hold when only the most fertile samples (Mg# ~0.90) in each xenolith suite are compared; thus, the differences in average Pd/Ir are not likely to be the result of biased sampling of only one type of xenolith. There is, however, no noticeable difference in Ir concentration, Re/Os ratios, or other PGE ratios between the xenolith localities. Thus, except for regional heterogeneities in Os and Pd, the remaining PGEs and Re appear to be rather homogeneous. The regional differences in Os and Pd content may reflect "primordial" upper mantle heterogeneities. If so, heterogeneities on very short length scales are required, because Oak Creek and Big Creek are only 100-km apart (Fig. 1). It is more likely, however, that these regional heterogeneities reflect complicated behaviors of the PGEs and Re during melting and/or during metasomatism as described in previous sections.

6. CONCLUSIONS

PGE-Re abundances and Re-Os isotopic compositions were determined for three suites of peridotite xenoliths in California. Ru/Ir ratios and Ir concentrations are constant over a wide range in S content and major-element fertility indices, indicating that Ru and Ir are compatible during partial melting and that their compatibilities are probably not controlled by the presence of sulfide. Pt/Ir, Pd/Ir, Os/Ir, and Re/Ir ratios range from slightly superchondritic to distinctly subchondritic for all xenoliths except for one anomalous sample (1026V), which is characterized by radiogenic $^{187}Os/^{188}Os$, low Re/Os ratio, and large enrichments in Cu, Os, Pt, Pd, and S relative to Ir (COPPS metasomatism). Assuming chondritic initial compositions, the magnitude of some of the depletions in Pt, Pd, Os, and Re requires incompatible behavior or substantial secondary loss. In detail, some samples, which are otherwise characterized by fertile major-element indices, exhibit low S contents and subchondritic Os/Ir and Pd/Ir ratios, indicating that depletions in Pd and Os relative to Ir are not a simple function of the degree of melting as inferred from major elements. Possible mechanisms for depleting Pt, Pd, Os, and Re relative to Ir include partitioning into chromian spinels and alloys, partitioning between sulfide and sulfide liquids, mobilization by aqueous fluids, and/or secondary loss associated with late-stage sulfide breakdown. It is not possible to explain all of the depletions in Pt, Pd, Os, and Re by any single mechanism.

The preferential enrichment in Os over Re and Ir in sample 1026V is somewhat paradoxical, because this sample's radiogenic $^{187}Os/^{188}Os$ requires a metasomatic agent originating from a source with a high time-integrated Re/Os ratio. The abundant garnet websterite xenoliths may be a suitable source, because they have high Re/Os ratios, radiogenic Os, and abundant garnet, which may sequester Re over Os during partial melting. However, their extremely low Os contents require the processing of huge amounts to concentrate enough Os into the metasomatic sulfides needed to enrich sample 1026V in Os. The homogeneity in $^{187}Os/^{188}Os$ ratio in the remaining xenoliths suggests that their Os isotopic compositions were not significantly affected by PGE metasomatism. The singular nature of 1026V's composition emphasizes the rarity of COPPS metasomatism. Finally, regional heterogeneities in Os/Ir and Pd/Ir ratios are likely to be due to complex depletion/enrichment processes, rather than to primordial mantle heterogeneities in PGE content.

Acknowledgments—Chemistry was done at Harvard University in 2001. Mass spectrometry was done at the California Institute of Technology. Thanks to K. Farley (Caltech) for making the ICP-MS available. A. Saunders and K. Sharkey are thanked for S analyses. D. Lange (Harvard) is thanked for help on the electron microprobe. B. Peucker-Ehrenbrink, D. Hassler, S. Jacobsen, W. McDonough, R. Rudnick, and Q. -Z. Yin provided useful discussions or insight on the fire assay technique and mass spectrometry. R. Rudnick is also thanked for some support (EAR 9909526). J. Chesley is thanked for insights on the glass vessel dissolution technique. S. Sorenson is thanked for access to some of the museum specimens, and R. Kistler is thanked for donating two samples. A. Brandon, E. Ripley, and an anonymous reviewer provided very helpful comments.

Associate editor: E. M. Ripley

REFERENCES

Alard O., Griffin W. L., Lorand J. P., Jackson S. E., and O'Reilly S. Y. (2000) Non-chondritic distribution of the highly siderophile elements in mantle sulfides. *Nature* **407,** 891–894.

Anders E. and Grevesse N. (1989) Abundances of the elements: Meteoritic and solar. *Geochim. Cosmochim. Acta* **53,** 197–214.

Baker D. R., Barnes S.-J., Simon G., and Bernier F. (2001) Fluid transport of sulfur and metals between sulfide melt and basaltic melt. *Can. Mineral.* **39,** 537–546.

Barnes S.-J., Naldrett A. J., and Gorton M. P. (1985) The origin of the fractionation of platinum-group elements in terrestrial magmas. *Chem. Geol.* **53,** 303–323.

Brandon A. D., Creaser R. A., Shirey S. B., and Carlson R. W. (1996) Osmium recycling in subduction zones. *Science* **272,** 861–864.

Brandon A. D., Walker R. J., Morgan J. W., Norman M. D., and Prichard H. M. (1998) Coupled ^{186}Os and ^{187}Os evidence for core-mantle interaction. *Science* **280,** 1570–1573.

Brandon A. D., Becker H., Carlson R. W., and Shirey S. B. (1999) Isotopic constraints on time scales and mechanisms of slab material transport in the mantle wedge: Evidence from the Simcoe mantle xenoliths, Washington, USA. *Chem. Geol.* **160,** 387–407.

Brenan J. M. and Andrews D. (2001) High-temperature stability of laurite and Ru-Os-Ir alloy and their role in PGE fractionation in mafic magmas. Can. Mineral. 39,341–360.

Brett R. (1984) Chemical equilibration of the Earth's core and upper mantle. *Geochim. Cosmochim. Acta* **48,** 1183–1188.

Capobianco C. J. and Drake M. J. (1990) Partitioning of ruthenium, rhodium, and palladium between spinel and silicate melt and implications for platinum group element fractionation trends. *Geochim. Cosmochim. Acta* **54,** 869–874.

Capobianco C. J., Hervig R. L., and Drake M. J. (1994) Experiments on crystal/liquid partitioning of Ru, Rh, and Pd for magnetite and hematite solid solutions crystallized from silicate melt. *Chem. Geol.* **113,** 23–43.

Chou C.-L. (1978) Fractionation of siderophile elements in the Earth's upper mantle. *Proc. Lunar Planet. Sci. C.* **9,** 219–230.

Crocket J. H., Fleet M. E., and Stone W. E. (1992) Experimental partitioning of osmium, iridium and gold between basalt melt and sulphide liquid at 1300°C. *Aust. J. Earth Sci.* **39,** 427–432.

Crocket J. H., Fleet M. E., and Stone W. E. (1997) Implications of composition for experimental partitioning of platinum-group elements and gold between sulfide liquid and basalt melt: The significance of nickel content. *Geochim. Cosmochim. Acta* **61,** 4139–4149.

Dickinson W. R. and Snyder W. S. (1978) Plate tectonics of the Laramide orogeny. In *Laramide Folding Associated with Basement Block Faulting in the Western United States* (ed. V. Matthews), Vol. Geol. Soc. Am. Mem. 151.

Dodge F. C. W., Lockwood J. P., and Calk L. C. (1988) Fragments of the mantle and crust beneath the Sierra Nevada batholith: Xenoliths in a volcanic pipe near Big Creek, California. *Geol. Soc. Am. Bull.* **100,** 938–947.

Ducea M. N. and Saleeby J. B. (1996) Buoyancy sources for a large, unrooted mountain range, the Sierra Nevada, California: Evidence from xenolith thermobarometry. *J. Geophys. Res.* **101,** 8229–8244.

Ducea M. N. and Saleeby J. B. (1998) The age and origin of a thick mafic-ultramafic keel from beneath the Sierra Nevada batholith. *Contrib. Mineral. Petr.* **133,** 169–185.

Ducea M. N. and Park S. K. (2000) Enhanced mantle conductivity from sulfide minerals, southern Sierra Nevada, California. *Geophys. Res. Lett.* **27,** 2405–2408.

Farmer G. L., Glazner A. F., Wilshire H. G., Wooden J. L., Pickthorn W. J., and Katz M. (1995) Origin of late Cenozoic basalts at the Cima volcanic field, Mojave Desert, California. *J. Geophys. Res.* **100,** 8399–8415.

Fleet M. E., Stone W. E., and Crocket J. H. (1991) Partitioning of palladium, iridium, and platinum between sulfide liquid and basalt melt: Effects of melt composition, concentration, and oxygen fugacity. *Geochim. Cosmochim. Acta* **55,** 2545–2554.

Fleet M. E., Chryssoulis S. L., Stone W. E., and Weisener C. G. (1993) Partitioning of platinum-group elements and Au in the Fe-Ni-Cu-S system: Experiments on the fractional crystallization of sulfide melt. *Contrib. Mineral. Petr.* **115,** 36–44.

Gueddari K., Piboule M., and Amosse J. (1996) Differentiation of platinum-group elements (PGE) and of gold during partial melting of peridotites in the lherzolitic massifs of the Betico-Rifean range (Ronda and Beni Bousera). *Chem. Geol.* **134,** 181–197.

Handler M. R. and Bennett V. C. (1999) Behaviour of platinum-group elements in the subcontinental mantle of eastern Australia during

variable metasomatism and melt depletion. *Geochim. Cosmochim. Acta* **63,** 3597–3618.
Handler M. R., Bennett V. C., and Dreibus G. (1999) Evidence from correlated Ir/Os and Cu/S for late-stage mobility in peridotite xenoliths: Implications for Re-Os systematics. *Geology* **27,** 75–78.
Jones J. H. and Drake M. J. (1986) Geochemical constraints on core formation in the Earth. *Nature* **322,** 221–228.
Kyte F. T., Smit J., and Wasson J. T. (1985) Siderophile interelement variations in the Cretaceous-Tertiary boundary sediments from Caravaca, Spain. *Earth Planet. Sci. Lett.* **73,** 183–195.
Lee C.-T. (2001) *The origin, evolution, and demise of continental lithospheric mantle: Perspectives from Re-Os isotopes, geochemistry, petrology, and modeling.* Harvard University, Ph.D. thesis.
Lee C.-T., Yin Q.-Z., Rudnick R. L., Chesley J. T., and Jacobsen S. B. (2000) Os isotopic evidence for Mesozoic removal of lithospheric mantle beneath the Sierra Nevada, California. *Science* **289,** 1912–1916.
Lee C-T., Rudnick R. L., Brimhall G. H. (2001a) Deep lithospheric dynamics beneath the Sierra Nevada during the Mesozoic and Cenozoic as inferred from xenolith petrology. Geochem. Geophy. Geosy. **2** (Paper number 2001GC000152).
Lee C.-T., Yin Q., Rudnick R. L., and Jacobsen S. B. (2001b) Preservation of ancient and fertile lithospheric mantle beneath the southwestern United States. *Nature* **411,** 69–73.
Lee C.-T., Yin Q.-Z., and Lee T.-C. (2001c) An internal normalization technique for unmixing total-spiked mixtures with application to MC-ICP-MS. *Comp. Geosci.* **27,** 577–581.
Legendere O. and Auge T. (1986) Mineralogy of platinum-group mineral inclusions in chromitites from different ophiolite complexes. In *Metallogeny of Basic and Ultrabasic Rocks* (ed. M. J. Gallagher et al., R. A. Ixer, C. R. Neary, and H. M. Prichard), pp. 361–375, Institute of Mining Metallurgy.
Lorand J. P. (1989) Mineralogy and chemistry of Cu-Fe-Ni sulfides in orogenic-type spinel peridotite bodies from Ariege (northeastern Pyrenees, France). *Contrib. Mineral. Petr.* **103,** 335–345.
Lorand J. P. (1990) Are spinel lherzolite xenoliths representative of the abundances of sulfur in the upper mantle? *Geochim. Cosmochim. Acta* **54,** 1487–1492.
Lorand J. P., Keays R. R., and Bodinier J. L. (1993) Copper and noble metal enrichments across the lithosphere-asthenosphere boundary of mantle diapirs: Evidence from the Lanzo Lherzolite Massif. *J. Petrol.* **34,** 1111–1140.
Lorand J.-P., Pattou L., and Gros M. (1999) Fractionation of platinum-group elements and gold in the upper mantle: a detailed study in Pyrenean orogenic lherzolites. *J. Petrol.* **40,** 957–981.
Lorand J.-P., Schmidt G., Palme H., and Kratz K.-L. (2000) Highly siderophile element geochemistry of the Earth's mantle: New data for the Lanzo (Italy) and Ronda (Spain) orogenic peridotite bodies. *Lithos* **53,** 149–164.
Luguet A., Alard O., Lorand J. P., Pearson N. J., Ryan C., and O'Reilly S. Y. (2001) Laser-ablation microprobe (LAM)-ICPMS unravels the highly siderophile element geochemistry of the oceanic mantle. *Earth Planet. Sci. Lett.* **189,** 285–294.
Maier W. D. and Barnes S.-J. (1999) Platinum-group elements in silicate rocks of the lower, critical and main zones at Union Section, western Bushveld Complex. *J. Petrol.* **40,** 1647–1671.
Maier W. D., Prichard H. M., Fisher P. C., and Barnes S.-J. (1999) Compositional variation of laurite at Union Section in the western Bushveld Complex. *S. Afr. J. Geol.* **102,** 286–292.
McInnes B. I. A., McBride J. S., Evans N. J., Lambert D. D., and Andrew A. S. (1999) Osmium isotope constraints on ore recycling in subduction zones. *Science* **286,** 512–516.
Meisel T., Walker R. J., and Morgan J. W. (1996) The osmium isotopic composition of the Earth's primitive upper mantle. *Nature* **383,** 517–520.
Morgan J. W. (1986) Ultramafic xenoliths: Clues to Earth's late accretionary history. *J. Geophys. Res.* **91,** 12375–12387.
Morgan J. W., Walker R. J., Brandon A. D., and Horan M. F. (2001) Siderophile elements in Earth's upper mantle and lunar breccias: Data synthesis suggests manifestations of the same late influx. *Meteorit. Planet. Sci.* **36,** 1257–1275.
Mukasa S. B. and Wilshire H. G. (1997) Isotopic and trace element compositions of upper mantle and lower crustal xenoliths, Cima volcanic field, California: Implications for evolution of the subcontinental lithospheric mantle. *J. Geophys. Res.* **102,** 20133–20148.
Mukhopadhyay B. and Manton W. I. (1994) Upper mantle fragments from beneath the Sierra Nevada batholith-partial fusion, fractional crystallization and metasomatism in subduction-related ancient lithosphere. *J. Petrol.* **35,** 1418–1450.
Murthy V. (1991) Early differentiation of the Earth and the problem of mantle siderophile elements: A new approach. *Science* **253,** 303–306.
Pattou L., Lorand J. P., and Gros M. (1996) Non-chondritic platinum-group element ratios in the Earth's mantle. *Nature* **379,** 712–715.
Peach C. L., Mathez E. A., Keays R. R., and Reeves S. J. (1994) Experimentally determined sulfide melt-silicate melt partition coefficients for iridium and palladium. *Chem. Geol.* **117,** 361–377.
Peslier A. H., Reisberg L., Ludden J., and Francis D. (2000) Re-Os constraints on harzburgite and lherzolite formation in the lithospheric mantle: A study of Northern Canadian Cordillera xenoliths. *Geochim. Cosmochim. Acta* **64,** 3061–3071.
Puchtel I. and Humayun M. (2000) Platinum group elements in Kostomuksha komatiites and basalts: Implications for oceanic crust recycling and core-mantle interaction. *Geochim. Cosmochim. Acta* **64,** 4227–4242.
Puchtel I. S. and Humayun H. (2001) Platinum group element fractionation in a komatiite basalt lava lake. *Geochim. Cosmochim. Acta* **65,** 2979–2993.
Rehkamper M., Halliday A. N., Barfod D., Fitton J. G., and Dawson J. B. (1997) Platinum-group element abundance patterns in different mantle environments. *Science* **278,** 1595–1598.
Rehkamper M., Halliday A. N., Alt J., Fitton J. G., Zipfel J., and Takazawa E. (1999) Non-chondritic platinum-group element ratios in oceanic mantle lithosphere: Petrogenetic signature of melt percolation? *Earth Planet. Sci. Lett.* **172,** 65–81.
Righter K. and Hauri E. H. (1998) Compatibility of rhenium in garnet during mantle melting and magma genesis. *Science* **280,** 1737–1741.
Righter K., Walker R. J., and Warren P. H. (2000) Significance of highly siderophile elements and osmium isotopes in the lunar and terrestrial mantles. In *Origin of the Earth and Moon* (ed. R. M. C. K. Righter), pp. 291–322, University of Arizona Press.
Roy-Barman M., Wasserburg G. J., Papnastassiou D. A., and Chaussidon M. (1998) Osmium isotopic compositions and Re-Os concentrations in sulfide globules from basaltic glasses. *Earth Planet. Sci. Lett.* **154,** 331–347.
Snow J. E. and Schmidt G. (1998) Constraints on Earth accretion deduced from noble metals in the oceanic mantle. *Nature* **391,** 166–169.
Walker R. J. and Morgan J. W. (1989) Rhenium-osmium isotope systematics of carbonaceous chondrites. *Science* **243,** 519–522.
Walker R. J., Carlson R. W., Shirey S. B., and Boyd F. R. (1989) Os, Sr, Nd, and Pb isotope systematics of southern African peridotite xenoliths: Implications for the chemical evolution of subcontinental mantle. *Geochim. Cosmochim. Acta* **53,** 1583–1595.
Wilshire H. G., McGuire A. V., Noller J. S., and Turrin B. D. (1991) Petrology of lower crustal and upper mantle xenoliths from the Cima volcanic field, California. *J. Petrol.* **32,** 169–200.
Wilson M. R., Kyser T. K., and Fagan R. (1996) Sulfur isotope systematics and platinum group element behavior in REE-enriched metasomatic fluids: A study of mantle xenoliths from Dish Hill, California, USA. *Geochim. Cosmochim. Acta* **60,** 1933–1942.
Wood S. A. (1987) Thermodynamic calculations of the volatility of the platinum group elements (PGE): The PGE content of fluids at magmatic temperatures. *Geochim. Cosmochim. Acta* **51,** 3041–3050.
Yin Q. Z., Jacobsen S. B., Lee C.-T., McDonough W. F., Rudnick R. L., and Horn I. (2001) A gravimetric K2OsCl6 standard: Application to precise and accurate Os spike calibration. *Geochim. Cosmochim. Acta* **65,** 2113–2127.

APPENDIX 1

Big Creek

BC77 spinel-garnet harzburgite

Porphyroclastic texture consisting of large orthopyroxene and clinopyroxene grains set in a fine-grained matrix of olivine, orthopyroxene, clinopyroxene, spinel, and garnet. Orthopyroxenes and clinopyroxenes show fine pyroxene exsolution lamellae. In some orthopyroxenes, the pyroxene exsolution lamellae have been replaced by amphibole. Orthopyroxenes also show abundant garnet exsolution lamellae. No visible sulfides were observed. Orthopyroxenes have high Ca, Al cores and low

Ca, Al rims (clinopyroxenes show reverse zonation). Garnet also occurs as discrete grains in the groundmass. Spinel is less abundant than garnet and occurs as two distinct populations. One population occurs as dark spinel grains within garnet coronae, and the other population occurs as tiny, apple-green grains surrounding garnet grains. The former has Cr/(Cr+Al) of 0.63 and the latter has Cr/(Cr+Al) of 0.30.

1026V spinel-garnet lherzolite

Porphyroclastic texture consisting of large orthopyroxene and clinopyroxene grains set in a fine-grained matrix of olivine, orthopyroxene, clinopyroxene, spinel, garnet, and sulfide. Orthopyroxenes and clinopyroxenes show fine pyroxene exsolution lamellae. Orthopyroxenes and clinopyroxenes show abundant garnet exsolution lamellae. Garnet lamellae in clinopyroxenes are much thicker those found in orthopyroxenes. Sulfides are abundant and occur as individual inclusions within olivines, groups of inclusions in healed/annealed fractures, or as discrete intergranular blebs. Included sulfides are monosulfide solid solution, pentlandite, or chalcopyrite, in some cases occurring simultaneously. Intergranular sulfides are also monosulfide solid solution, pentlandite and/or chalcopyrite (up to 200 microns in size) but are typically broken down into low-temperature assemblages, such as millerite and Fe-oxides and Fe-hydroxides. Orthopyroxenes have high Ca, Al cores and low Ca, Al rims (clinopyroxenes show reverse zonation). Garnet also occurs as discrete grains in the groundmass. Spinel occurs as two distinct populations. One population occurs as dark spinel grains within garnet coronae, and the other population occurs as tiny, apple-green grains surrounding garnet grains. The former has Cr/(Cr+Al) of 0.56 to 63 and the latter has Cr/(Cr+Al) of 0.08. Sulfide compositions are shown in Table A1.

P1 spinel lherzolite

No thin section was available for this sample.

P6 spinel-garnet lherzolite

Equigranular fabric made up of orthopyroxene, clinopyroxene, olivine, spinel, garnet, and rare Fe-oxides. No visible sulfides. Spinels (Cr/(Cr+Al) = 0.3–0.5) occur as isolated grains or as grains surrounded by garnet grains. Some garnets have thin opaque rims. Orthopyroxenes show zoning from high Ca, Al cores to low Ca, Al rims (clinopyroxene shows reverse zonation).

P7 spinel lherzolite

Equigranular fabric made up of orthopyroxene, clinopyroxene, olivine, spinel, and minor amphibole. No visible sulfides. Pyroxenes show fine pyroxene exsolution lamellae. Orthopyroxenes are zoned from high Ca cores to low Ca rims, while clinopyroxenes show reverse zonation. Spinels are amber in color, large (up to 3 mm), and are not zoned (Cr/(Cr+Al) = 0.17). One amphibole was found in thin section and was observed as a replacement product of orthopyroxene.

P10 spinel lherzolite

Equigranular fabric made up of orthopyroxene, clinopyroxene, olivine, and spinel (Cr/(Cr+Al) = 0.34). No visible sulfides. Orthopyroxenes are zoned from high Ca cores to low Ca rims, while clinopyroxenes show reverse zonation. Partial serpentinization on grain boundaries.

BC98-2 spinel harzburgite

Equigranular fabric made up of orthopyroxene, clinopyroxene, olivine, and spinel. Orthopyroxenes have low Ca cores and high Ca rims (clinopyroxene shows reverse zonation). No visible sulfides. Spinels are dark brown and have Cr/(Cr+Al) between 0.5 and 0.7.

BC98-1 garnet websterite

Large equigranular grains, consisting of garnet, clinopyroxene, orthopyroxene, and olivine in decreasing abundance, respectively. Garnet occurs as large round grains. No visible sulfide.

Oak Creek

OK98-2 spinel lherzolite

Fine-grained, granular groundmass of olivine, orthopyroxene, clinopyroxene, and spinel. There is an overall subtle foliation texture and the occasional presence of large olivine grains, showing undulatory extinction. Minerals are chemically homogeneous. Spinels are Al-rich (Cr/(Cr+Al) = 0.30). No visible sulfides.

OK98-3 spinel lherzolite

Fine-grained, granular groundmass of olivine, orthopyroxene, clinopyroxene, and spinel. There is an overall subtle foliation texture and the occasional presence of large olivine grains, showing undulatory extinction. Minerals are chemically homogeneous. Spinels are Al-rich (Cr/(Cr+Al) = 0.09). No visible sulfides.

OK984 spinel lherzolite

Fine-grained, granular groundmass of olivine, orthopyroxene, clinopyroxene, and spinel. There is an overall subtle foliation texture and the occasional presence of large olivine grains, showing undulatory extinction. Minerals are chemically homogeneous. Spinels are Al-rich (Cr/(Cr+Al) = 0.10). No visible sulfides.

Cima

Ki5-16 spinel harzburgite

Coarse-grained groundmass of olivine, orthopyroxene, minor clinopyroxene, and spinel. No visible sulfides.

Ki5-139 plagioclase-bearing spinel lherzolite

Fine-grained groundmass of olivine, orthopyroxene, clinopyroxene, spinel, and plagioclase. No visible sulfides. Plagioclase grains almost invariably surrounded by fine-grained, olivine-spinel coronae.

Ki5-32 spinel harzburgite

Fine-grained groundmass of olivine, orthopyroxene, clinopyroxene, and amber-colored spinel. Sulfides abundant as tiny grains in healed or annealed fractures in olivine. There are occasional opaque minerals, presumed to be Fe oxides.

CiP98-64 spinel harzburgite

Coarse-grained groundmass of olivine, orthopyroxene, minor clinopyroxene, and spinel. No visible sulfides.

San Carlos

SC99-1 spinel lherzolite

Coarse-grained groundmass of olivine, clinopyroxene, orthopyroxene, and spinel. No visible sulfides.

Appendix Table A1.

		S	Fe	Co	Ni	Cu	Total
Sulfide 1-inclusion in olivine							
1	mss	38.44	33.21	0.77	26.87	0.05	99.34
2	mss	32.79	27.54	0.76	38.40	0.29	99.78
3	mss	38.71	33.55	0.78	26.34	0.00	99.38
4	mss	33.24	27.18	0.77	38.67	0.24	100.10
5	cp	34.41	38.51	0.20	2.01	23.47	98.60
6	cp	34.27	33.90	0.14	1.58	28.60	98.49
7	cp	34.60	37.21	0.16	2.28	24.59	98.84
Sulfide 2-intergranular							
8	mi	28.93	0.26	0.51	67.92	0.65	98.27
9	mi	29.84	0.38	0.63	66.76	0.72	98.33
11	mi	28.28	0.56	0.43	68.50	0.57	98.34
Sulfide 5-intergranular							
14	mi	34.66	2.34	0.78	61.15	1.63	100.56
15	mi	34.58	2.13	0.78	61.12	1.57	100.18
Sulfide 6-intergranular							
16	mss?	36.46	20.70	0.66	41.43	0.14	99.39
17	mss?	36.93	21.29	0.64	40.82	0.21	99.89
18	cp	34.18	30.29	0.13	3.39	30.99	98.98
19	cp	34.07	30.40	0.12	2.99	31.16	98.74

All compositions in wt %, monosulfide solid solution (mss), chalcopyrite (cp), millerite (mi)